

Antipodal Identification in Reissner-Nordström Spacetime

Nathaniel A. Strauss* and Bernard F. Whiting†

Department of Physics, University of Florida, Gainesville, Florida, USA

Anne T. Franzen‡

*Center for Mathematical Analysis, Geometry and Dynamical Systems,
Mathematics Department, Instituto Superior Técnico, Universidade de Lisboa, Lisbon, Portugal*

(Dated: February 25, 2020)

We extend the discussion of the antipodal identification of black holes to the Reissner-Nordström (RN) spacetime. We solve the massless Klein-Gordon equation in the RN background in terms of scattering coefficients and provide a procedure for constructing a solution for an arbitrary analytic extension of RN. The behavior of the maximally extended solution is highly dependent upon the coefficients of scattering between the inner and outer horizons, so we present the low-frequency behavior of, and numerical solutions for, these quantities. We find that, for low enough frequency, field amplitudes of solutions with purely positive or negative frequency at each horizon will acquire only a phase after passing both the inner and outer horizons, while at higher frequencies the amplitudes will tend to grow exponentially either to the future or to the past, and decay exponentially in the other direction. Regardless, we can always construct a complete basis of globally antipodal symmetric and antisymmetric solutions for any finite analytic extension of RN. We have characterized this basis in terms of positive and negative frequency solutions so that they could be used to begin constructing the corresponding quantum field theory.

arXiv:2002.02501v2 [gr-qc] 22 Feb 2020

* straussn@ufl.edu

† bernard@phys.ufl.edu

‡ anne.franzen@tecnico.ulisboa.pt

CONTENTS

I. Introduction	3
II. The Reissner-Nordström Manifold	4
A. Spherical Coordinates	4
B. Kruskal-Szekeres Coordinates	4
III. Solving the Klein-Gordon Equation	6
A. Separation of Variables	7
B. Solutions in Each Spacetime Region	8
1. Regions I and I'	8
2. Regions II and II'	8
3. Regions III and III'	8
C. Building Global Solutions	11
1. An Extended Reissner-Nordström Solution	11
2. A Maximally Extended Reissner-Nordström Solution	11
IV. Scattering Coefficients in Region II	13
A. Low Frequency	13
B. Numerical Series Solution	16
V. Linearly Independent and Symmetric Fields	17
A. Linear Independence of Positive and Negative Frequency Solutions	17
B. A complete basis of solutions	18
C. Constructing a basis of symmetric and antisymmetric solutions	19
VI. Discussion	20
Acknowledgements	20
References	21
A. Positive and Negative Frequency Solutions	22

I. INTRODUCTION

Antipodal identification is the physical identification of, or a mapping between, two regions of spacetime on a manifold, where the precise meaning of “antipodal” varies by the manifold. Interest in antipodal identification began in the construction of quantum field theory (QFT) in four-dimensional de Sitter space, proposed by Schrödinger in 1957 and explicitly developed by Sanchez in 1987 [1, 2]. In this so called “elliptic interpretation” two spacelike separated points are physically identified as a single space point with the future light cone of one of the points coinciding with the past light cone of the other point. As has subsequently been noticed by Gibbons and others, the “elliptic interpretation”, which may arise in connection with discussions on topology change [3, 4], could have an impact on quantum mechanics [5], can lead to lack of time orientation [6] and the absence of a spinor structure [7], and can result in causality violation [8]. Nevertheless, Sanchez proposed a QFT for this model in terms of antipodal symmetric fields, though not requiring the states to have symmetry. This is finally compared to scenarios without identified points. She had used these ideas earlier in a collaboration with Castagnino et al., in which they investigated constant curvature, self-consistent solutions of semiclassical Einstein equations [9]. Further, together in Domenech et al., they extend this analysis for anti-de Sitter and Rindler spacetimes [10]. Later, Stephens supported the antipodal identification in Rindler spacetimes by demonstrating its importance in the interpretation of pair production in a uniform electric field [11]. Friedman and Higuchi then explained how time non-orientable QFT can be constructed locally in antipodally identified de Sitter spacetime by viewing the spacetime as a four-dimensional Möbius strip [12]. In contrast to [2], they employ antipodally symmetric algebraic states on de Sitter space. Alternatively, Chang and Li found that de Sitter spacetime with antipodal identification is in fact orientable in odd dimensions, and they explicitly construct the resulting QFT [13].

The discussion of antipodal identification becomes much richer in black hole spacetimes, and most of the discussion so far has been confined to the Schwarzschild (charge-neutral, non-rotating) black hole. In concurrence with work on de Sitter space, motivated by unconventional ideas of ’t Hooft [14, 15], Sanchez and Whiting [16] explicitly constructed a globally antipodally symmetric scalar field on the Schwarzschild manifold. They found that the usual Fock space construction is not possible and the usual thermal features are not present (although Martellini and Sanchez have proposed a

construction which circumvents this difficulty [17]). Subsequently, Whiting discussed the effect of these explicit representations of symmetric fields on the role of gravitation in thermal physics [18]. More recently, ’t Hooft has suggested an antipodal identification of the Schwarzschild black hole motivated by the quantum information paradox [19–22]. The resulting unusual structure of spacetime restores quantum pureness and time reversal symmetry, properties usually not seen in thermodynamic objects. In [19] he first proposes that unitarity should be assumed as a crucial guiding principle, which leads to a topology of Schwarzschild spacetime different from the one usually assumed. According to ’t Hooft, Hawking radiation is only locally thermal. Globally however, quantum states evolve purely unitarily, assuming an entanglement of each particle in the first exterior with a partner appearing in the second exterior, and similarly for particles in the interior. He refers to this entanglement as antipodal identification. ’t Hooft also explains how this causes a topological twist of the background metric and even removes firewalls [20]. He explains this in more detail in [21], while a shorter review of the idea is given in [22]. The effects of this entanglement on black hole scattering and vacuum states has been investigated [23, 24]. Antipodal identification has also found recent support in the construction of theories of quantum gravity [25, 26]. In sum, it has been shown that antipodal identification has a large effect on the quantum and thermal features of black holes.

The contribution of this paper is to extend the discussion of antipodal identification to the Reissner-Nordström (RN) spacetime, that of a charged, non-rotating black hole. Proceeding in the same manner as Sanchez and Whiting [16], we solve the massless Klein-Gordon equation on the RN background, and we construct antipodal symmetric fields in terms of positive- and negative-frequency solutions, which could be used in the antipodal identification of the corresponding QFT. Two primary difficulties arise. First, the presence of more than one horizon requires the consideration of more than one antipodal identification on the analytic extension of the RN geometry. Constructing symmetric fields about a single horizon is analogous to the Schwarzschild case. Constructing a solution simultaneously symmetric about multiple horizons is also possible if we utilize solutions with positive frequency at one horizon and negative frequency at another horizon. Second, the amplitude of a solution in an arbitrary analytic extension is highly dependent upon the scattering coefficients for propagation between the two horizons of RN. For this reason we examine the low-frequency limit of these coefficients, as well as their values ob-

tained from a numerical series approximation. We find that for certain frequency ranges of the scalar field, and especially at high frequency, the amplitude of the field diverges as it propagates through the maximally extended geometry. Despite this fact, antipodal identification is possible for an analytic extension of any finite number of horizons.

The structure of the paper is as follows. In Sec. II, we introduce the RN manifold and its Kruskal-Szekeres coordinates. Further, we specify its characteristic regions separated by outer and inner horizons and show their representation in Penrose diagrams. In Sec. III we solve the massless Klein-Gordon equation in each spacetime region and demonstrate how to build global solutions. In Sec. IV, we present the low frequency limits of, and numerical solutions for, the coefficients of scattering between the two RN horizons. In Sec. V we discuss the linear independence of Klein-Gordon solutions in an analytical extension of RN and demonstrate how to construct symmetric fields from these solutions. Finally, in Sec. VI we summarize and discuss our results.

II. THE REISSNER-NORDSTRÖM MANIFOLD

The physics of any spacetime manifold is determined by the metric $g_{\mu\nu}(x)$ and its derivatives, and the Einstein equations relate $g_{\mu\nu}$ to the distribution of matter:

$$R_{\mu\nu} - \frac{1}{2}Rg_{\mu\nu} = 8\pi T_{\mu\nu}, \quad (1)$$

where $R_{\mu\nu}$ is the Ricci tensor, R is the curvature scalar, $g_{\mu\nu}$ is the metric, and $T_{\mu\nu}$ is the stress-energy tensor. The Schwarzschild metric is a spherically symmetric non-trivial vacuum ($T_{\mu\nu} = 0$) solution to Eq. 1, representing a charge-neutral, non-rotating black hole. The RN manifold is a generalization of the Schwarzschild manifold that allows for a spherically symmetric electromagnetic field. The assumption of spherical symmetry is retained from the Schwarzschild derivation, but on the right hand side one uses the electromagnetic stress energy tensor:

$$T_{\mu\nu} = F_{\mu\rho}F_{\nu}{}^{\rho} - \frac{1}{4}g_{\mu\nu}F_{\rho\sigma}F^{\rho\sigma}, \quad (2)$$

where $F_{\mu\nu}$ is the electromagnetic field tensor [27]. If we assume no magnetic monopoles are present, the only non-vanishing component of the electromagnetic field tensor is $F^{tr} = -F^{rt} = Q/r^2$ in spherical coordinates [27]. Solving the resulting Einstein equations yields the RN manifold, which describes a charged, non-rotating black hole.

In the following sections, we examine the properties of the RN manifold in both standard spherical coordinates and in Kruskal coordinates, each of which provide valuable physical intuition for the structure of the RN manifold and the behavior of nearby particles.

A. Spherical Coordinates

The RN metric outlined above in standard spherical coordinates is

$$g_{\mu\nu}dx^{\mu}dx^{\nu} = -f(r)dt^2 + f(r)^{-1}dr^2 + r^2d\theta^2 + r^2\sin^2\theta d\phi^2, \quad (3)$$

where

$$f(r) = 1 - \frac{2M}{r} + \frac{Q^2}{r^2} = \frac{(r-r_+)(r-r_-)}{r^2}, \quad (4)$$

where

$$r_{\pm} = M \pm \sqrt{M^2 - Q^2}. \quad (5)$$

We interpret M as the mass and Q as the charge of the black hole. We recover the Schwarzschild manifold at $Q = 0$.

We see that the g_{rr} component of the metric is singular at $r = 0, r_{\pm}$. The singularity at $r = 0$ is a geometric singularity as in the Schwarzschild case, $r = r_+$ is the outer event horizon (corresponding to the Schwarzschild horizon since $r_+ \rightarrow 2M$ as $Q \rightarrow 0$), and $r = r_-$ is a Cauchy horizon (which has no Schwarzschild analog, since $r_- \rightarrow 0$ as $Q \rightarrow 0$ and vanishes completely when $Q = 0$).

Qualitatively speaking, classical geodesics in this spacetime have different behavior from those of a Schwarzschild black hole. After crossing r_+ from the outside, uncharged particles inevitably move inward, as in the Schwarzschild case. However, after crossing r_- , the singularity repels the particle and the particle's geodesic again crosses r_- , after which the particle inevitably exits r_+ again, ejected into a new external world [27].

B. Kruskal-Szekeres Coordinates

In the following we will introduce two sets of Kruskal-Szekeres coordinates, each of which is regular at one of the horizons. First, we define the so-called tortoise coordinate r_* :

$$\frac{dr_*}{dr} = \frac{1}{f(r)}, \quad (6)$$

and when integrated

$$\begin{aligned} r_* &= \int_0^r \frac{dr'}{(1 - \frac{r_+}{r'}) (1 - \frac{r_-}{r'})} \\ &= r + \frac{1}{2\kappa_+} \ln \left| \frac{r}{r_+} - 1 \right| - \frac{1}{2\kappa_-} \ln \left| \frac{r}{r_-} - 1 \right|, \end{aligned} \quad (7)$$

where

$$\kappa_{\pm} = \frac{1}{2} \left(\frac{r_+ - r_-}{r_{\pm}^2} \right) \quad (8)$$

are the surface gravities at the outer and inner horizons, defined here to be positive. Note the following corresponding limits of r and r_* :

$$\begin{array}{c} r \rightarrow |-\infty| 0 |r_-| r_+ | \infty \\ r_* \rightarrow |-\infty| 0 | \infty | -\infty | \infty. \end{array} \quad (9)$$

There are two sets of Kruskal-Szekeres coordinates for the RN geometry, one regular at each horizon. We keep the coordinates θ and ϕ , while transforming t and r into new coordinates U and V . The (partial) set of coordinates regular at the outer horizon is

$$\begin{aligned} U_+ &= \begin{cases} e^{\kappa_+(r_*-t)} & r > r_+ \\ -e^{\kappa_+(r_*-t)} & r_- < r < r_+ \end{cases}, \\ V_+ &= e^{\kappa_+(r_*+t)}. \end{aligned}$$

The change in sign of U_+ at r_+ keeps the coordinate transformation one-to-one. We call the spacetime region where $r > r_+$ region I and the spacetime region where $r_- < r < r_+$ region II. We can also introduce a sign change in the V_+ coordinate, where the negative values of V correspond to another universe with its own r and t coordinates. We have then created two new spacetime regions I' and II', as seen in Fig. 1. In order to line up the corresponding boundaries of the primed and unprimed universes, we also need to introduce a sign change in U_+ for the primed universe. The full set of Kruskal-Szekeres coordinates centered at the outer horizon is then

$$U_+ = \begin{cases} e^{\kappa_+(r_*-t)} & \text{I, II}' \\ -e^{\kappa_+(r_*-t)} & \text{I}', \text{II} \end{cases}, \quad (10)$$

$$V_+ = \begin{cases} e^{\kappa_+(r_*+t)} & \text{I, II} \\ -e^{\kappa_+(r_*+t)} & \text{I}', \text{II}' \end{cases}. \quad (11)$$

The range of both U_+ and V_+ is $-\infty$ to ∞ . However, we can define new coordinates $\tilde{U}_+ = \tanh U_+$ and $\tilde{V}_+ = \tanh V_+$, which each range from -1 to 1 . This allows us to visualize the RN spacetime by drawing a Penrose diagram (see Fig. 1).

Similarly, the set of coordinates regular at the in-

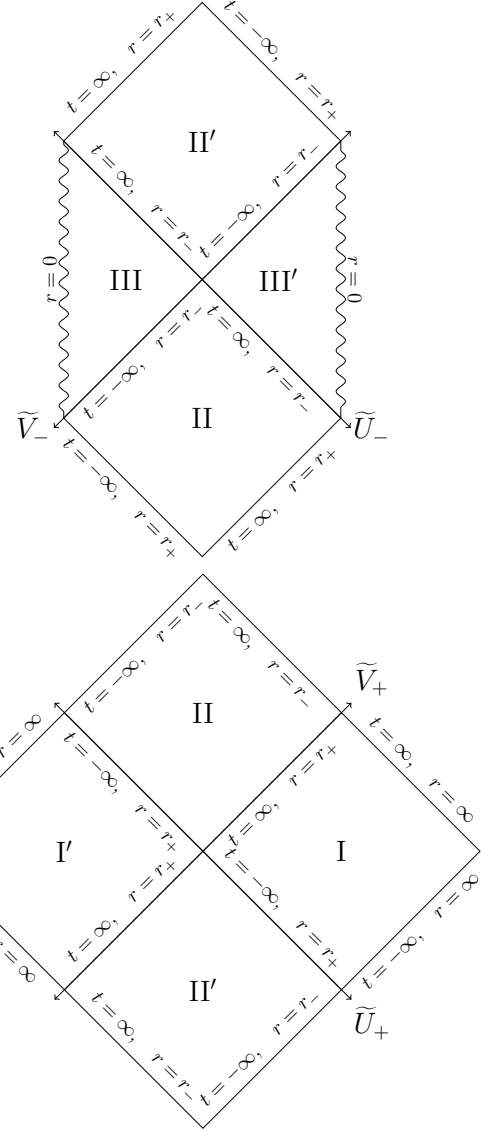


FIG. 1. These are the Penrose diagrams for the RN spacetime regions in the $\tilde{U}_- \tilde{V}_-$ -plane (above) and $\tilde{U}_+ \tilde{V}_+$ -plane (below). The $r = 0$ curve in the $\tilde{U}_- \tilde{V}_-$ -plane is represented as a squiggly vertical line, though its true shape is some other curve in the $\tilde{U}_- \tilde{V}_-$ -plane.

ner horizon is

$$U_- = \begin{cases} e^{-\kappa_-(r_*-t)} & \text{II, III}' \\ -e^{-\kappa_-(r_*-t)} & \text{II}', \text{III} \end{cases} \quad (12)$$

$$V_- = \begin{cases} e^{-\kappa_-(r_*+t)} & \text{II, III} \\ -e^{-\kappa_-(r_*+t)} & \text{II}', \text{III}' \end{cases}. \quad (13)$$

The range of U_- and V_- is not the whole real line, since the lower limit $r = 0$ is a curve in $U_- V_-$ -

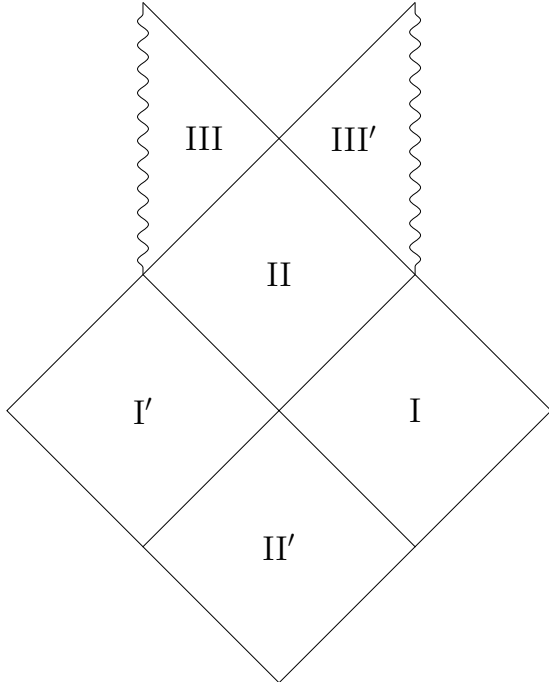


FIG. 2. The Penrose diagram for regions in an analytically extended RN spacetime.

space, beyond which U_- and V_- are not defined. Nevertheless, we can still define $\tilde{U}_- = \tanh U_-$ and $\tilde{V}_- = \tanh V_-$. The Penrose diagram for the RN spacetime in these coordinates is shown in Fig. 1.

Using these coordinates, we can construct an extended RN spacetime with arbitrarily many spacetime regions. Shown in Fig. 2 is what we call a single extended RN spacetime, which contains two asymptotically flat regions or universes. You may notice that region II is covered by both the U_+V_+ - and U_-V_- -coordinates. Shown in Fig. 3 is a section of a maximal analytic extension of the RN spacetime.

III. SOLVING THE KLEIN-GORDON EQUATION

Now that we have two convenient coordinate systems to cover the RN manifold, we can work towards defining a quantum field theory. The goal of this paper is to solve the massless Klein-Gordon equation, which is the classical field equation for a massless scalar field, leaving the definition of the corresponding field operators to future work. While we cannot find analytic solutions, we can characterize a basis of two linearly independent solutions for each spacetime region in terms of scattering coefficients. We can then use these bases to construct global solutions for an analytic extension of RN.

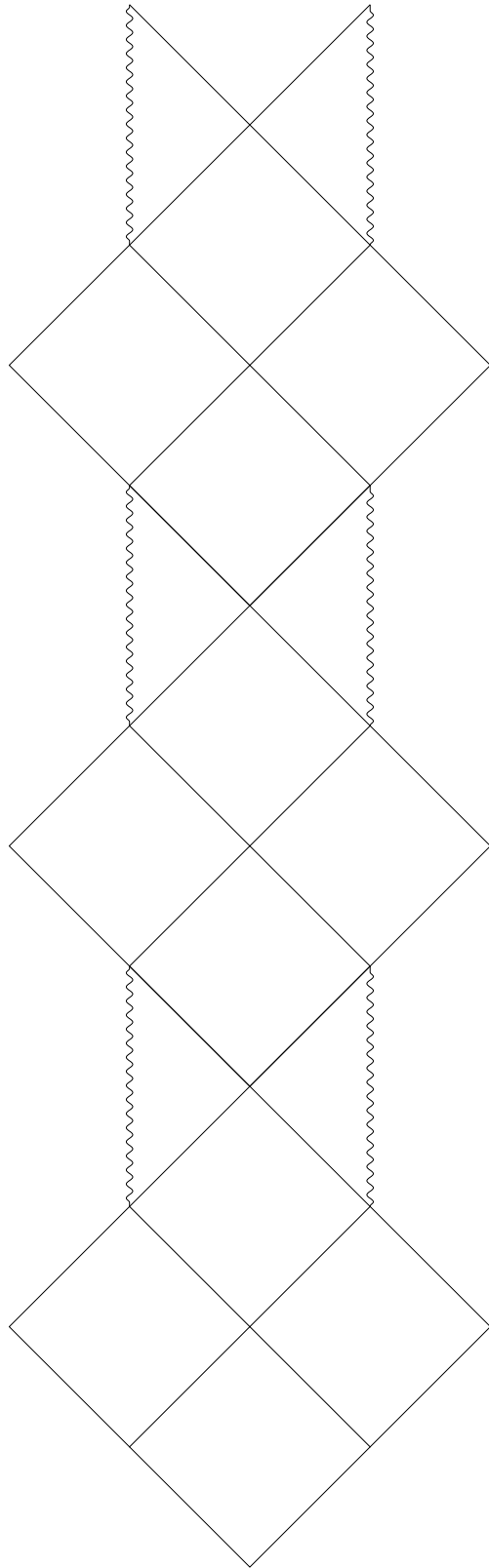


FIG. 3. A section of the Penrose diagram for a maximal analytic extension of the RN spacetime, which proceeds infinitely in both directions.

A. Separation of Variables

In this section we use the method of separation of variables on the Klein-Gordon equation, showing that the limiting behavior of the solution is that of a spherical wave. The Klein-Gordon equation in a general spacetime metric g for a massless scalar field φ is

$$\square\varphi \equiv \frac{1}{\sqrt{-g}}\partial_\mu(\sqrt{-g}g^{\mu\nu}\partial_\nu\varphi) = 0, \quad (14)$$

where $g = \det g_{\mu\nu}$. For the RN spacetime in spherical coordinates,

$$g = -r^4 \sin^2 \theta, \quad (15)$$

and so using the RN spacetime in Eq. 14,

$$\begin{aligned} \square\varphi = & -\frac{1}{f}\partial_t^2\varphi + \frac{1}{r^2}\partial_r(r^2f\partial_r\varphi) \\ & + \frac{1}{r^2\sin\theta}\partial_\theta(\sin\theta\partial_\theta\varphi) + \frac{1}{r^2\sin^2\theta}\partial_\phi^2\varphi. \end{aligned} \quad (16)$$

Using the method of separation of variables, we define $\varphi(t, r, \theta, \phi) = T(t)R(r)Y(\theta, \phi)$. Applying this to the Klein-Gordon equation,

$$\begin{aligned} 0 = & -\frac{1}{T}\frac{r^2}{f}\partial_t^2T + \frac{1}{R}\partial_r(r^2f\partial_rR) \\ & + \frac{1}{Y}\left(\frac{1}{\sin\theta}\partial_\theta(\sin\theta\partial_\theta Y) + \frac{1}{\sin^2\theta}\partial_\phi^2Y\right) \end{aligned} \quad (17)$$

This successfully separates the t and r dependence from the angular dependence.

Eq. 17 implies that the angular part must be equal to a constant, which we call $-l(l+1)$:

$$\begin{aligned} -l(l+1) = & \\ & (1/Y_l)\left(\frac{1}{\sin\theta}\partial_\theta(\sin\theta\partial_\theta Y_l) + \frac{1}{\sin^2\theta}\partial_\phi^2 Y_l\right) \end{aligned} \quad (18)$$

We can perform a further separation of variables, which yields the familiar spherical harmonics:

$$\begin{aligned} Y_l(\theta, \phi) = & \sum_{m=-l}^l \alpha_{lm} Y_l^m(\theta, \phi) \\ = & \sum_{m=-l}^l \alpha_m \sqrt{\frac{(2l+1)(l-m)!}{4\pi(l+m)!}} \\ & \cdot P_l^m(\cos\theta)e^{im\phi}, \end{aligned} \quad (19)$$

where Y_l^m are the spherical harmonics, P_l^m are the

associated Legendre polynomials, and the α_{lm} are constants.

Substituting Eq. 18 into Eq. 17, we have

$$-\frac{1}{T}\partial_t^2T + \frac{1}{R}\frac{f}{r^2}\partial_r(r^2f\partial_rR) - \frac{l(l+1)}{r^2}f = 0. \quad (20)$$

This separates the time part from the radial part, implying that the time part must be equal to a constant, which we call ω^2 :

$$-\frac{1}{T}\partial_t^2T = \omega^2. \quad (21)$$

We use the solution

$$T(t) = e^{-i\omega t}. \quad (22)$$

So far, we've found the angular and time parts of a solution to the Klein-Gordon equation of the form $\varphi = e^{-i\omega t}R(r)Y_l^m(\theta, \phi)$. To find $R(r)$, we substitute Eq. 21 into Eq. 20 to obtain an ordinary differential equation for $R(r)$:

$$\frac{1}{R}\frac{f}{r^2}\partial_r(r^2f\partial_rR) - \frac{l(l+1)}{r^2}f + \omega^2 = 0, \quad (23)$$

where $f(r)$ is given in Eq. 4. Note that, as an equation in r , Eq. 23 has regular singular points at $r = r_-$ and $r = r_+$, and an irregular singular point of rank 1 at $r = \infty$. Note also that, as seen from Eq. 9, r_* diverges at all three singular points.

To simplify Eq. 23 further, we introduce a new function

$$A(r) = \frac{r}{r_+}R(r). \quad (24)$$

The r_+ is an arbitrarily chosen constant in order to preserve units. In terms of $A(r)$, Eq. 23 becomes

$$f\partial_r(f\partial_rA) + \left(-\frac{f}{r}(\partial_r f) - \frac{l(l+1)}{r^2}f + \omega^2\right)A = 0. \quad (25)$$

Now we can change variables to the tortoise coordinate r_* (see Eq. 6), and we finally have

$$\frac{d^2A(r_*)}{dr_*^2} - (V_{\text{eff}}(r) - \omega^2)A(r_*) = 0, \quad (26)$$

where

$$V_{\text{eff}} = \frac{f}{r}(\partial_r f) + \frac{l(l+1)}{r^2}f \quad (27)$$

is the effective potential.

While we cannot write Eq. 26 explicitly in terms of r_* , we have reduced the radial equation to a time-independent Schrödinger-type equation. In particu-

lar, $V_{\text{eff}} \rightarrow 0$ as $r \rightarrow r_{\pm}, \infty$. This means that the two linearly independent solutions near the boundaries (singular points) $r = r_{\pm}$ and $r \rightarrow \infty$ are

$$R(r_*) \rightarrow \begin{cases} \frac{r_{\pm}}{r} e^{+i\omega r_*} \\ \frac{r_{\pm}}{r} e^{-i\omega r_*} \end{cases} \quad \text{as } r \rightarrow r_+, r_-, \infty. \quad (28)$$

Even though we have not analytically solved the Klein-Gordon equation, we have enough information to single out solutions with unique limiting behavior. Note that, as r_* diverges at all three of these limits, the radial solution infinitely oscillates near each of these boundaries, approaching a constant amplitude as $r \rightarrow r_{\pm}$, and decreasing in amplitude as $r \rightarrow \infty$. At this point, we can begin characterizing solutions in each spacetime region in terms of scattering coefficients.

B. Solutions in Each Spacetime Region

In Section III A, we showed that near the horizons and at spatial infinity, the solution to the Klein-Gordon equation is a spherical wave. Since Eq. 26 is a homogeneous second-order ordinary differential equation, a basis for the solution space has two solutions for each spacetime region I, II, and III. In this section, we specify the boundary conditions for each solution in each spacetime region.

1. Regions I and I'

Regions I and I' are identical except for a reversal in the flow of the Killing vector field ∂_t . This results in a simple 180 degree rotation in the Penrose diagram, so the same basis of solutions will work for both regions. For the first basis solution, we specify the boundary condition $R_I \rightarrow T e^{-i\omega r_*}$ as $r \rightarrow r_+$. This means that the r_+ horizon emits no waves. T is chosen so that when this boundary condition propagates to infinity,

$$R_I = \begin{cases} \frac{r_{\pm}}{r} T e^{-i\omega r_*} & r \rightarrow r_+ \\ \frac{r_{\pm}}{r} (e^{-i\omega r_*} + R e^{i\omega r_*}) & r \rightarrow \infty \end{cases}. \quad (29)$$

The choice of 1 as the coefficient of $e^{-i\omega r_*}$ inside the bracket provides the second boundary condition and a scale for this solution.

We can see from Eq. 26, which is real when r and ω are real, that R_I^* is another, linearly independent solution, which we take to be our second basis solu-

tion (unless $T = 0$):

$$R_I^* = \begin{cases} \frac{r_{\pm}}{r} T^* e^{i\omega r_*} & r \rightarrow r_+ \\ \frac{r_{\pm}}{r} (R^* e^{-i\omega r_*} + e^{i\omega r_*}) & r \rightarrow \infty \end{cases}. \quad (30)$$

This solution has no waves entering the future r_+ horizon, and can be viewed as a time-reversed R_I . Recalling that the time part is $T(t) = e^{-i\omega t}$, we can distinguish the ingoing and outgoing parts and thus visualize these solutions as in Fig. 4.

We can now use the Wronskian to find a relation between these scattering coefficients. Since Eq. 26 has no first-order derivatives, the Wronskian $W(\frac{r}{r_+} R_I, \frac{r}{r_+} R_I^*)$ is constant in r_* . We calculate

$$\begin{aligned} W(\frac{r}{r_+} R_I, \frac{r}{r_+} R_I^*)|_{r \rightarrow \infty} &= 2i\omega(1 - |R|^2) \\ W(\frac{r}{r_+} R_I, \frac{r}{r_+} R_I^*)|_{r \rightarrow r_+} &= 2i\omega|T|^2. \end{aligned}$$

This implies that

$$|T|^2 + |R|^2 = 1, \quad (31)$$

which we interpret as conservation of energy.

2. Regions II and II'

Similarly to Region I, we specify the boundary condition $R_{II} \rightarrow \hat{T} e^{-i\omega r_*}$ as $r \rightarrow r_+$ and let the solution propagate to $r = r_-$. This solution and its complex conjugate form a basis of solutions for regions II and II', as shown in Fig. 5.

Again, we can use the Wronskian to find a relation between the scattering coefficients:

$$\begin{aligned} W(\frac{r}{r_+} R_{II}, \frac{r}{r_+} R_{II}^*)|_{r \rightarrow r_+} &= 2i\omega|\hat{T}|^2, \\ W(\frac{r}{r_+} R_{II}, \frac{r}{r_+} R_{II}^*)|_{r \rightarrow r_-} &= 2i\omega(1 - |\hat{R}|^2), \end{aligned}$$

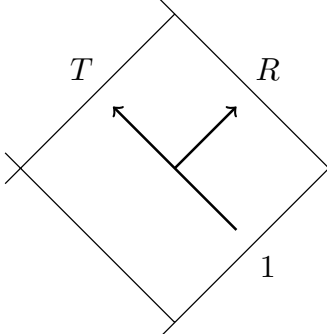
and thus

$$|\hat{T}|^2 + |\hat{R}|^2 = 1. \quad (32)$$

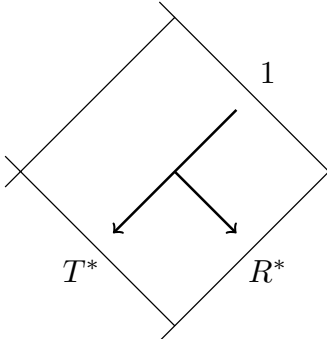
Note that this consequence of the Wronskian relation depends on the choice of basis in region II and may not be standard. For example, in [28], a choice different from our Fig. 5 is made, and a relation different from (but equivalent to) Eq. 32 is obtained.

3. Regions III and III'

As we've already determined, $R(r) \rightarrow e^{\pm i\omega r_*}$ as $r \rightarrow r_-$, but it is not immediately clear from Eq. 26 how $R(r)$ behaves as $r \rightarrow 0$, since V_{eff} diverges there

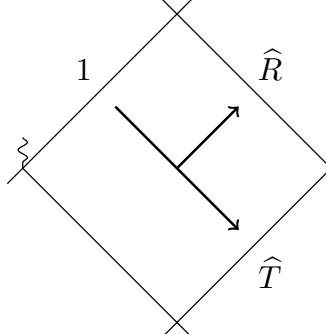


$$R_{\text{I}} = \begin{cases} \frac{r_{\pm}}{r} T e^{-i\omega r_*} & r \rightarrow r_+ \\ \frac{r_{\pm}}{r} (e^{-i\omega r_*} + R e^{i\omega r_*}) & r \rightarrow \infty \end{cases}$$

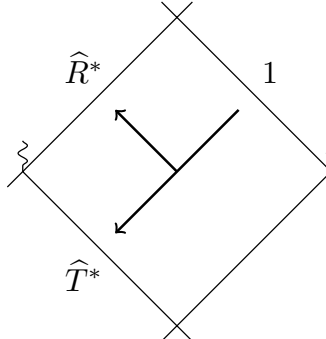


$$R_{\text{I}}^* = \begin{cases} \frac{r_{\pm}}{r} T^* e^{i\omega r_*} & r \rightarrow r_+ \\ \frac{r_{\pm}}{r} (R^* e^{-i\omega r_*} + e^{i\omega r_*}) & r \rightarrow \infty \end{cases}$$

FIG. 4. A basis of solutions for region I.



$$R_{\text{II}} = \begin{cases} \frac{r_{\pm}}{r} (e^{-i\omega r_*} + \widehat{R} e^{i\omega r_*}) & r \rightarrow r_- \\ \frac{r_{\pm}}{r} \widehat{T} e^{-i\omega r_*} & r \rightarrow r_+ \end{cases}$$



$$R_{\text{II}}^* = \begin{cases} \frac{r_{\pm}}{r} (\widehat{R}^* e^{-i\omega r_*} + e^{i\omega r_*}) & r \rightarrow r_- \\ \frac{r_{\pm}}{r} \widehat{T}^* e^{i\omega r_*} & r \rightarrow r_+ \end{cases}$$

FIG. 5. A basis of solutions for region II.

and the definition of $A(r)$ breaks down. In fact, we have to return to the radial equation in the form of Eq. 23 to test the regularity or singularity of the scalar wave equation at $r = 0$. We can rewrite the equation in the form

$$\frac{d^2 R}{dr^2} + \frac{\partial_r(r^2 f)}{r^2 f} \frac{dR}{dr} + \left(-\frac{l(l+1)}{r^2 f} + \frac{\omega}{f^2} \right) R = 0. \quad (33)$$

Now, in the limit of $r \rightarrow 0$,

$$\begin{aligned} \frac{\partial_r(r^2 f)}{r^2 f} &\rightarrow -\frac{2M}{Q^2}, \\ -\frac{l(l+1)}{r^2 f} + \frac{\omega}{f^2} &\rightarrow -\frac{l(l+1)}{Q^2}. \end{aligned}$$

Since both of these limits are finite, $r = 0$ is a regular point of the radial equation, despite being a geometric singularity. Taking a Taylor series about this point, the two linearly independent behaviors

as $r \rightarrow 0$ are $R \rightarrow 1, r/r_-$. Here r_- is arbitrarily chosen to preserve units. We use these as boundary conditions to obtain our basis of solutions for region III.

In addition, since $r = 0$ is a regular point of the field equation, if necessary we can append a space-time with negative r . Where $r < 0$ there are no horizons, so the spacetime has a naked singularity [29]. The boundary conditions “scatter” from the singularity as shown in Fig. 6. We can use the Wronskian along with the definition Eq. 6 to find a relation between $A, B, C,$ and D :

$$\begin{aligned} W\left(\frac{r}{r_+} R_{\text{III},1}, \frac{r}{r_+} R_{\text{III},r}\right)|_{r \rightarrow r_-} &= 2i\omega(A^* B - AB^*), \\ W\left(\frac{r}{r_+} R_{\text{III},1}, \frac{r}{r_+} R_{\text{III},r}\right)|_{r \rightarrow -\infty} &= 2i\omega(C^* D - CD^*), \\ W\left(\frac{r}{r_+} R_{\text{III},1}, \frac{r}{r_+} R_{\text{III},r}\right)|_{r \rightarrow 0} &= \frac{(r-r_+)(r-r_-)}{r_+^2 r_-} \\ &\rightarrow \frac{1}{r_+}, \end{aligned}$$

FIG. 6. A basis of solutions for region III.

and so we have

$$AB^* - A^*B = CD^* - C^*D = \frac{i}{2r_+\omega}. \quad (34)$$

If we are unconcerned with the behavior at $r = 0$, but would still like to append a geometry with negative r , it might be convenient to introduce an alternative basis for region III, which specifies boundary conditions at $r = r_-$ and $r = -\infty$ instead of at $r = 0$. Such a basis is given in Fig 7. Computing the Wronskians, we find the relationships between the scattering coefficients \tilde{T} , \tilde{R} , A , B , C , and D :

$$W\left(\frac{r}{r_+}R_{\text{III}}, \frac{r}{r_+}R_{\text{III}}^*\right)\Big|_{r \rightarrow -\infty} = 2i\omega|\tilde{T}|^2$$

$$W\left(\frac{r}{r_+}R_{\text{III}}, \frac{r}{r_+}R_{\text{III}}^*\right)\Big|_{r \rightarrow r_-} = 2i\omega(1 - |\tilde{R}|^2)$$

FIG. 7. An alternative basis of solutions for region III.

$$W\left(\frac{r}{r_+}R_{\text{III}}, \frac{r}{r_+}R_{\text{III},1}\right)\Big|_{r \rightarrow -\infty} = 2i\omega\tilde{T}C$$

$$W\left(\frac{r}{r_+}R_{\text{III}}, \frac{r}{r_+}R_{\text{III},1}\right)\Big|_{r \rightarrow r_-} = 2i\omega(A - \tilde{R}A^*)$$

$$W\left(\frac{r}{r_+}R_{\text{III}}, \frac{r}{r_+}R_{\text{III},r}\right)\Big|_{r \rightarrow -\infty} = 2i\omega\tilde{T}D$$

$$W\left(\frac{r}{r_+}R_{\text{III}}, \frac{r}{r_+}R_{\text{III},r}\right)\Big|_{r \rightarrow r_-} = 2i\omega(B - \tilde{R}B^*).$$

Solving the above systems of equations, we derive the following relations:

$$1 = |\tilde{T}|^2 + |\tilde{R}|^2, \quad (35)$$

$$\tilde{T} = \frac{AB^* - A^*B}{B^*C - A^*D}, \quad (36)$$

$$\tilde{R} = \frac{BC - AD}{B^*C - A^*D}. \quad (37)$$

We now have a basis of solutions for every space-time region in an arbitrarily extended RN manifold. In the next section, we demonstrate how to put these together into a global solution.

C. Building Global Solutions

In the previous section we constructed a basis of solutions to the Klein-Gordon equation in a single spacetime region. We will now use this basis to build a global basis of solutions for the manifold shown in Fig. 2 as well as a maximally extended RN spacetime shown in Fig. 3.

1. An Extended Reissner-Nordström Solution

We will now construct a global solution of positive frequency for the extended RN spacetime shown in Fig. 2. The result is shown in Fig. 8, but the first step to obtain this solution is to specify a boundary condition within a single spacetime region. It will be convenient to specify radiation at only one of the inner horizon boundaries in region II'. In region II', this solution is a linear combination of R_{II} and R_{II}^* :

$$R(r)|_{\text{II}'} = -\frac{\widehat{R}^*}{|\widehat{T}|^2} R_{\text{II}} + \frac{1}{|\widehat{T}|^2} R_{\text{II}}^*. \quad (38)$$

The propagation of a solution across the outer horizon (i.e. across the U_+ - or V_+ -axis) requires consideration of the analyticity of the solution on the horizon. There are two solutions analytical at the horizon for a given solution in region I. At the point $(-\widetilde{U}_+, -\widetilde{V}_+)$ in region I', the value of the so-called ‘‘positive frequency’’ solution is $1/K_+$ times the value at the point $(\widetilde{U}_+, \widetilde{V}_+)$ in region I, where

$$K_{\pm} = e^{\pi\omega/\kappa_{\pm}}. \quad (39)$$

For negative frequency solutions, the multiplicative factor is K_+ . Similarly at the inner horizon, at the point $(\widetilde{U}_-, -\widetilde{V}_-)$ in region III', the value of the positive frequency solution is $1/K_-$ times the value at the point $(-\widetilde{U}_-, \widetilde{V}_-)$. For negative frequency solutions, the multiplicative factor is K_- . See Appendix A for the definitions of the positive and negative frequency solutions.

Proceeding by choosing positive frequency at both horizons and finding the correct linear combination for region II, we find the propagation in Fig. 8. The boundaries at $r = 0$ and $r = -\infty$ can be found by taking the correct linear combinations of the solutions in Figs. 6 and 7, but the expressions are complicated and irrelevant to our analysis of maximally extended solutions below. At this point, we have constructed a global solution to a single extended RN geometry from two boundary conditions and two frequency choices (one at each horizon).

2. A Maximally Extended Reissner-Nordström Solution

One could continue the process outlined in the previous section in order to construct a solution in a maximally extended RN geometry (see Fig. 3), but beyond a single extended RN geometry, the expressions get long and complicated. Instead, we will formulate the propagation of the scalar field through single RN geometries as an eigenvalue problem in the two-dimensional space of solutions with positive frequency at every horizon. We can then determine the amplitude of the scalar field arbitrarily far from the boundary conditions.

After fixing positive frequency at all horizons, there are two linearly independent global solutions for the entire maximally extended RN geometry. We choose the two solutions ϕ_1 and ϕ_2 shown in Fig. 9, whose domains are now the maximally extended RN manifold. The set $\{\phi_1, \phi_2\}$ forms a basis for the linear space of globally positive frequency solutions, so we can write any solution $\phi = \alpha_0\phi_1 + \beta_0\phi_2$, where α_0 and β_0 are the boundary conditions for ϕ on the inner horizon in region II'.

Using the amplitudes of ϕ_1 and ϕ_2 shown in Fig. 9, we find that on the inner horizon of region II of the n^{th} extended RN geometry (proceeding upwards), the amplitudes α_n and β_n are

$$\begin{pmatrix} \alpha_n \\ \beta_n \end{pmatrix} = M_{++}^n \begin{pmatrix} \alpha_0 \\ \beta_0 \end{pmatrix}, \quad (40)$$

where

$$M_{++} \equiv \begin{pmatrix} K_- \left(\frac{1}{K_+} - K_+ |\widehat{R}|^2 \right) \frac{1}{|\widehat{T}|^2} & K_- \left(K_+ - \frac{1}{K_+} \right) \frac{\widehat{R}}{|\widehat{T}|^2} \\ -\frac{1}{K_-} \left(K_+ - \frac{1}{K_+} \right) \frac{\widehat{R}^*}{|\widehat{T}|^2} & \frac{1}{K_-} \left(K_+ - \frac{1}{K_+} |\widehat{R}|^2 \right) \frac{1}{|\widehat{T}|^2} \end{pmatrix}. \quad (41)$$

The evolution of the field depends entirely upon the properties of the matrix M_{++} (where the two positive signs stand for positive frequency at both horizons). Using the Wronskian relation Eq. 32, we find

$$\det M_{++} = 1 \quad (42)$$

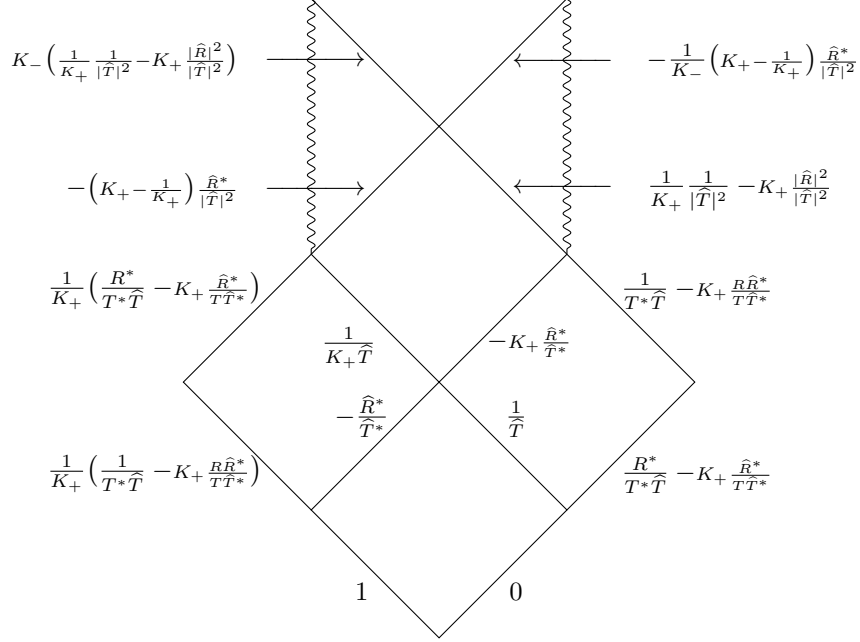


FIG. 8. A representation of a global, positive frequency solution for an extended RN geometry.

and

$$\begin{aligned}
& \text{tr } M_{++} \\
&= \frac{K_+}{K_-} + \frac{K_-}{K_+} - \left(K_+ - \frac{1}{K_+}\right) \left(K_- - \frac{1}{K_-}\right) \frac{|\widehat{R}|^2}{|\widehat{T}|^2} \\
&= 2 \cosh 4\pi\omega M - 4 \frac{|\widehat{R}|^2}{|\widehat{T}|^2} \sinh(\pi\omega/\kappa_+) \sinh(\pi\omega/\kappa_-) \\
&= \frac{2}{|\widehat{T}|^2} \left(\cosh 4\pi\omega M - |\widehat{R}|^2 \sinh \pi\omega(1/\kappa_+ + 1/\kappa_-) \right).
\end{aligned} \tag{43}$$

Since $\det M_{++} > 0$, M_{++} is invertible, M_{++}^{-1} exists, and we can propagate the field “downwards” with M_{++}^{-1} . Using the eigenvalue equation, we can find the eigenvalues λ_{\pm} and the associated eigenvectors $\vec{\lambda}_{\pm}$:

$$\lambda_{\pm} = \frac{1}{2} \text{tr } M_{++} \pm \sqrt{\left(\frac{1}{2} \text{tr } M_{++}\right)^2 - 1} \tag{44}$$

$$\vec{\lambda}_{\pm} = \begin{pmatrix} K_-(K_+ - \frac{1}{K_+}) \frac{\widehat{R}}{|\widehat{T}|^2} \\ \lambda_{\pm} - K_-(\frac{1}{K_+} - K_+ |\widehat{R}|^2) \end{pmatrix} \tag{45}$$

$$\propto \begin{pmatrix} \lambda_{\pm} - \frac{1}{K_-} (K_+ - \frac{1}{K_+}) |\widehat{R}|^2 \\ -\frac{1}{K_-} (K_+ - \frac{1}{K_+}) \frac{\widehat{R}}{|\widehat{T}|^2} \end{pmatrix}. \tag{46}$$

Now let us discuss these results. While at this point we know nothing about the M , Q , and ω dependence of \widehat{R} and \widehat{T} , the eigenvalues depend only on the quantity $\frac{1}{2} \text{tr } M_{++}$. If $(\frac{1}{2} \text{tr } M_{++})^2 < 1$, we have that $\lambda_{\pm} \notin \mathbb{R}$, $\lambda_+ = \lambda_-^*$, and $|\lambda_{\pm}|^2 = 1$. In this situation we have the desirable property that the amplitude of the solution is non-divergent as one proceeds arbitrarily far upwards or downwards in the maximally extended geometry. If $(\frac{1}{2} \text{tr } M_{++})^2 = 1$, then $\lambda_{\pm} \in \mathbb{R}$ and $\lambda_+ = \lambda_- = 1$. However, we also have that $\vec{\lambda}_+ = \vec{\lambda}_-$, which means that M_{++} has become a defective matrix with a double eigenvalue but only a single eigenvector. Thus, the solution associated with this eigenvector will not diverge, but all other solutions will diverge. Lastly, if $(\frac{1}{2} \text{tr } M_{++})^2 > 1$, then $\lambda_{\pm} \in \mathbb{R}$, $\lambda_{\pm} \neq 1$, and $\lambda_+ = 1/\lambda_-$. In this case, the amplitude of the solutions corresponding to λ_{\pm} will diverge in one direction and converge to zero in the other direction. Any superposition of these two solutions will diverge in both directions.

Clearly the first case is the most desirable as it is the only case where no solutions diverge. A necessary and sufficient condition for a non-divergent solution space is

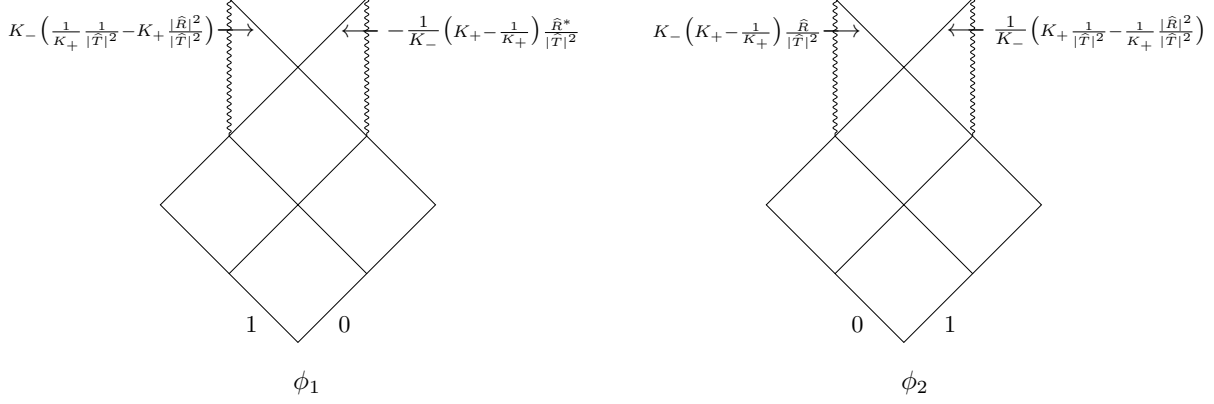


FIG. 9. Any positive-frequency solution to a single extended RN geometry can be written in the basis of the solutions ϕ_1 and ϕ_2 above.

$$|\frac{1}{2} \text{tr } M_{++}| < 1 \quad (47)$$

$$\iff \frac{\sinh^2(2\pi\omega M)}{\sinh(\pi\omega/\kappa_+) \sinh(\pi\omega/\kappa_-)} < \frac{|\widehat{R}|^2}{|\widehat{T}|^2} < \frac{\cosh^2(2\pi\omega M)}{\sinh(\pi\omega/\kappa_+) \sinh(\pi\omega/\kappa_-)} \quad (48)$$

$$\iff \frac{\sinh 2\pi\omega M}{\sinh \pi\omega(1/2\kappa_+ + 1/2\kappa_-)} < |\widehat{R}| < \frac{\cosh 2\pi\omega M}{\cosh \pi\omega(1/2\kappa_+ + 1/2\kappa_-)}. \quad (49)$$

In order to determine if or when this condition is satisfied, we need to know the dependence of \widehat{R} and \widehat{T} on M , ω , Q , and l . In the next section, we provide analytical and numerical approximations to answer this question.

IV. SCATTERING COEFFICIENTS IN REGION II

As we saw in the previous section, the global structure of a scalar field on a maximally extended RN manifold is highly dependent on the scattering coefficients for region II, \widehat{T} and \widehat{R} . We cannot solve for these analytically, but we can solve the low-frequency limit analytically. We also provide a nu-

merically obtained example to demonstrate the limitations of the low-frequency solution.

A. Low Frequency

In this section, we will obtain expressions for the scattering coefficients for region II in the low frequency limit. To do this, we arrange the radial equation in a form similar to Euler's hypergeometric equation, drop higher order terms in order to match to the hypergeometric equation, and find \widehat{T} and \widehat{R} using the scattering properties of the hypergeometric function.

To begin, we define a re-scaled radial coordinate $x = (r - r_-)/(r_+ - r_-)$, in terms of which the radial equation Eq. 23 becomes

$$0 = \left(\frac{d^2}{dx^2} + (r_+ - r_-)^2 \omega^2 + \frac{1}{x} \left(\frac{1}{2} + l(l+1) - \frac{r_+^4 - 2r_+^3 r_- - 2r_+ r_-^3 + r_-^4}{(r_+ - r_-)^2} \omega^2 + (r_+^2 - r_-^2) \omega^2 \right) \right. \\ \left. + \frac{1}{1-x} \left(\frac{1}{2} + l(l+1) - \frac{r_+^4 - 2r_+^3 r_- - 2r_+ r_-^3 + r_-^4}{(r_+ - r_-)^2} \omega^2 - (r_+^2 - r_-^2) \omega^2 \right) \right. \\ \left. + \frac{1}{x^2} \left(\frac{1}{4} + \frac{r_-^4 \omega^2}{(r_+ - r_-)^2} \right) + \frac{1}{(1-x)^2} \left(\frac{1}{4} + \frac{r_+^4 \omega^2}{(r_+ - r_-)^2} \right) \right) \sqrt{x(1-x)} R(x). \quad (50)$$

At this point, we need to drop the terms $(r_+ - r_-)^2\omega^2$ and $(r_+^2 - r_-^2)\omega^2$, which can be accomplished by imposing $M\omega \ll 1$. Doing so, we rearrange to find

$$0 = \left(\frac{d^2}{dx^2} + \frac{1}{x(1-x)} \left(\frac{1}{2} + l(l+1) - \frac{r_+^4 - 2r_+^3r_- - 2r_+r_-^3 + r_-^4}{(r_+ - r_-)^2} \omega^2 \right) \right. \\ \left. + \frac{1}{x^2} \left(\frac{1}{4} + \frac{r_-^4\omega^2}{(r_+ - r_-)^2} \right) + \frac{1}{(1-x)^2} \left(\frac{1}{4} + \frac{r_+^4\omega^2}{(r_+ - r_-)^2} \right) \right) \sqrt{x(1-x)} R(x). \quad (51)$$

The hypergeometric equation for the hypergeometric function $F(a, b, c; z)$ can be written in the form

$$0 = \left(\frac{d^2}{dz^2} + \frac{1}{z(1-z)} \left(\frac{1}{4} + \left(\frac{a-b}{2} \right)^2 - \left(\frac{c-1}{2} \right)^2 - \left(\frac{a+b-c}{2} \right)^2 \right) \right. \\ \left. + \frac{1}{z^2} \left(\frac{1}{4} - \left(\frac{c-1}{2} \right)^2 \right) + \frac{1}{(1-z)^2} \left(\frac{1}{4} - \left(\frac{a+b-c}{2} \right)^2 \right) \right) \cdot z^{c/2} (1-z)^{(1+a+b-c)/2} F(a, b, c; z). \quad (52)$$

We can now see that the radial equation and the hypergeometric equation are in similar forms. Because the radial solution of interest is

$$R_{\text{II}} \xrightarrow[r \rightarrow r_+]{\frac{r_+}{r}} \widehat{T} e^{-i\omega r_*} = \frac{r_+}{r} \widehat{T} e^{-i\omega r} \left(\frac{r_+ - r_-}{r_+} \right)^{-\frac{i\omega r_+^2}{r_+ - r_-}} \left(\frac{r_+ - r_-}{r_-} \right)^{\frac{i\omega r_-^2}{r_+ - r_-}} (1-x)^{-\frac{i r_+^2 \omega}{r_+ - r_-}} x^{\frac{i r_-^2 \omega}{r_+ - r_-}}, \quad (53)$$

we find it useful to make the substitution $z = 1 - x$, which means the radial solution is related to the hypergeometric function by

$$R(x) = (1-x)^{(c-1)/2} x^{(a+b-c)/2} F(a, b, c; 1-x). \quad (54)$$

With this substitution, in comparing Eqs. 52 and 51 we can make the identifications

$$\frac{c-1}{2} = -i \frac{\omega r_+^2}{r_+ - r_-} = -i\omega/2\kappa_+ \quad (55)$$

$$\frac{a+b-c}{2} = +i \frac{\omega r_-^2}{r_+ - r_-} = +i\omega/2\kappa_- \quad (56)$$

$$\frac{a-b}{2} = \frac{1}{2} \sqrt{(2l+1)^2 - 8(r_+^2 + r_+r_- + r_-^2)\omega^2}. \quad (57)$$

The sign choices in Eqs. 55 and 56 were made to match Eq. 54 to Eq. 53, and the sign choice in Eq. 57 is arbitrary since it only interchanges a and b . Solving the above system of equations, we find

$$a = \frac{1}{2} \left(1 - 2i\omega(r_+ + r_-) + \sqrt{(1+2l)^2 - 8(r_+^2 + r_+r_- + r_-^2)\omega^2} \right) \quad (58)$$

$$b = \frac{1}{2} \left(1 - 2i\omega(r_+ + r_-) - \sqrt{(1+2l)^2 - 8(r_+^2 + r_+r_- + r_-^2)\omega^2} \right) \quad (59)$$

$$c = 1 - \frac{2ir_+^2\omega}{r_+ - r_-} = 1 - i\omega/\kappa_+. \quad (60)$$

Now that we have found a , b , and c , we can use Eqs. 53 and 54 to approximate the solution R_{II} found in Fig. 5:

$$R_{\text{II}} \approx C \widehat{T} (1-x)^{(c-1)/2} x^{(a+b-c)/2} F(a, b, c; 1-x), \quad (61)$$

where C is a constant phase, which can be calculated from Eq. 53. Then, according to the formula [30]

$$F(a, b, c; z) = \frac{\Gamma(c)\Gamma(c-a-b)}{\Gamma(c-a)\Gamma(c-b)} F(a, b, a+b-c+1; 1-z) + (1-z)^{-(a+b-c)} z^{-(c-1)} \frac{\Gamma(c)\Gamma(a+b-c)}{\Gamma(a)\Gamma(b)} F(1-a, 1-b, c-a-b+1; 1-z), \quad (62)$$

where Γ is the gamma function, we also have

$$R_{\text{II}} \approx C\widehat{T}(1-x)^{(c-1)/2} x^{(a+b-c)/2} \frac{\Gamma(c)\Gamma(c-a-b)}{\Gamma(c-a)\Gamma(c-b)} \cdot F(a, b, a+b-c+1; x) + C\widehat{T}(1-x)^{-(c-1)/2} x^{-(a+b-c)/2} \frac{\Gamma(c)\Gamma(a+b-c)}{\Gamma(a)\Gamma(b)} F(1-a, 1-b, c-a-b+1; x). \quad (63)$$

We can now calculate the limit as $x \rightarrow 0$:

$$R_{\text{II}} \xrightarrow[r \rightarrow r_-]{\approx} C\widehat{T} x^{\frac{r_-^2 \omega}{r_+ - r_-}} \frac{\Gamma(c)\Gamma(c-a-b)}{\Gamma(c-a)\Gamma(c-b)} + C\widehat{T} x^{-\frac{r_-^2 \omega}{r_+ - r_-}} \frac{\Gamma(c)\Gamma(a+b-c)}{\Gamma(a)\Gamma(b)} = CD\widehat{T} \frac{\Gamma(c)\Gamma(c-a-b)}{\Gamma(c-a)\Gamma(c-b)} e^{-i\omega r_*} + CD^*\widehat{T} \frac{\Gamma(c)\Gamma(a+b-c)}{\Gamma(a)\Gamma(b)} e^{i\omega r_*} \quad (64)$$

$$R_{\text{II}} \xrightarrow[r \rightarrow r_-]{} \frac{r_+}{r_-} (e^{-i\omega r_*} + \widehat{R} e^{i\omega r_*}), \quad (65)$$

where D is another constant phase, which can be calculated from Eq. 53. Comparing the last two lines, we conclude

$$\frac{1}{|\widehat{T}|} = \frac{r_-}{r_+} \left| \frac{\Gamma(c)\Gamma(c-a-b)}{\Gamma(c-a)\Gamma(c-b)} \right|, \quad \frac{|\widehat{R}|}{|\widehat{T}|} = \frac{r_-}{r_+} \left| \frac{\Gamma(c)\Gamma(a+b-c)}{\Gamma(a)\Gamma(b)} \right|. \quad (66)$$

Using the recursive relations $\Gamma(z) = \Gamma(z+1)/z = (z-1)\Gamma(z-1)$ and Euler's reflection formula $\Gamma(1-z)\Gamma(z) = \pi/\sin(\pi z)$, we can find compact expressions for the low-frequency limits of $|\widehat{T}|^2$ and $|\widehat{R}|^2$:

$$|\widehat{T}|^2 = \frac{2 \sinh(2\pi\omega \frac{r_+^2}{r_+ - r_-}) \sinh(2\pi\omega \frac{r_-^2}{r_+ - r_-})}{\cosh(2\pi\omega \frac{r_+^2 + r_-^2}{r_+ - r_-}) + \cos(2\pi\sqrt{(l + \frac{1}{2})^2 - 2\omega^2(r_+^2 + r_+ r_- + r_-^2)})}, \quad (67)$$

$$|\widehat{R}|^2 = \frac{\cosh(2\pi\omega \frac{r_+^2 - r_-^2}{r_+ - r_-}) + \cos(2\pi\sqrt{(l + \frac{1}{2})^2 - 2\omega^2(r_+^2 + r_+ r_- + r_-^2)})}{\cosh(2\pi\omega \frac{r_+^2 + r_-^2}{r_+ - r_-}) + \cos(2\pi\sqrt{(l + \frac{1}{2})^2 - 2\omega^2(r_+^2 + r_+ r_- + r_-^2)})}. \quad (68)$$

One can check that $|\widehat{T}|^2 + |\widehat{R}|^2 = 1$ as expected. In addition, if we take the limit $\omega \rightarrow 0$ in the above expressions for $|\widehat{T}|^2$ and $|\widehat{R}|^2$, we find

$$|\widehat{T}| \rightarrow \frac{2r_+ r_-}{r_+^2 + r_-^2} = \frac{Q^2}{2M^2 - Q^2} \quad (69)$$

$$|\widehat{R}| \rightarrow \frac{r_+^2 - r_-^2}{r_+^2 + r_-^2} = \frac{2M\sqrt{M^2 - Q^2}}{2M^2 - Q^2}. \quad (70)$$

Interestingly, it is not the case that $|\widehat{T}| \rightarrow 0$ as $\omega \rightarrow 0$, as might naively be expected for the exterior region. This result is consistent with that of [28], where the corresponding scattering coefficients

in the interior are uniformly bounded.

We will now apply Eqs. 67 and 68 to the discussion at the end of Section III C 2. Note that Eq. 68 is minimized when the cosine is equal to -1 , which occurs if we assume small enough ω to drop the ω^2 term under the square root. The resulting $|\widehat{R}|^2$ corresponds exactly to the case $\frac{1}{2} \text{tr} M_{++} = 1$ (see Eq. 49). Thus, in the low-frequency regime without dropping the ω^2 term under the square root, the value of $|\widehat{R}|^2$ deviates slightly above the lower limit of Eq. 49. Thus, we conclude that the solution space of a maximal analytic extension of RN is non-divergent in the low-frequency limit. In the next section, we use a numer-

ical series solution method to determine whether a non-divergent solution space also exists at mid- to high-frequencies.

B. Numerical Series Solution

In this section, we use the Frobenius method outlined in Bender and Orszag [31] to obtain numerical results for the scattering coefficients \hat{T} and \hat{R} . We expand the radial function $R(r)$ about the singular points $r = r_+$ and $r = r_-$ with the same boundary conditions as the radial mode R_{II} found in Fig. 5. By matching the solutions at $r = M$, which is always between the two horizons, we can find numerical results for $|\hat{T}|^2$ and $|\hat{R}|^2$.

We begin by proposing an ansatz, which is an expansion about the regular singular point $r = r_+$ or $r = r_-$:

$$R(r - r_{\pm}) = (r - r_{\pm})^{\alpha} \sum_{n=0}^{\infty} a_n (r - r_{\pm})^n, \quad (71)$$

where α is an unspecified constant called the indicial exponent, and the a_n are constant coefficients. We then plug Eq. 71 into Eq. 23, and collect terms in powers of $r - r_{\pm}$. The coefficient of each power of $r - r_{\pm}$ must be equal to zero in order to satisfy the resulting equation. By setting the coefficient of $(r - r_{\pm})^{\alpha-2}$ equal to zero, we find two solutions for the indicial exponent:

$$\alpha = +i \frac{\omega r_{\pm}^2}{r_+ - r_-}, \quad (72)$$

$$\alpha = -i \frac{\omega r_{\pm}^2}{r_+ - r_-}. \quad (73)$$

Using the indicial exponent in Eq. 72, we can see from Eq 53 that $(r - r_-)^{\alpha}$ is proportional to $e^{-i\omega r_*}$ when expanding about $r = r_-$, and $(r - r_+)^{\alpha}$ is proportional to $e^{+i\omega r_*}$ when expanding about $r = r_+$. We then set $a_0 = 1$ and set the remaining coefficients of $(r - r_{\pm})^{\alpha+n-2}$ equal to zero, which results in a five-term recurrence relation for the remaining a_n . When numerically evaluating the series in Eq. 71, we find that the terms exponentially converge to the exact solution. Thus, we can safely numerically evaluate the derivative:

$$R'(r - r_{\pm}) = (r - r_{\pm})^{\alpha} \sum_{n=0}^{\infty} a_n n (r - r_{\pm})^{n-1}. \quad (74)$$

Furthermore, the radius of convergence is at least as large as the distance to the next singular point of Eq. 23, so expansions about $r = r_-$ and $r = r_+$

$|\hat{T}|^2$ and $|\hat{R}|^2$ vs. $M\omega$

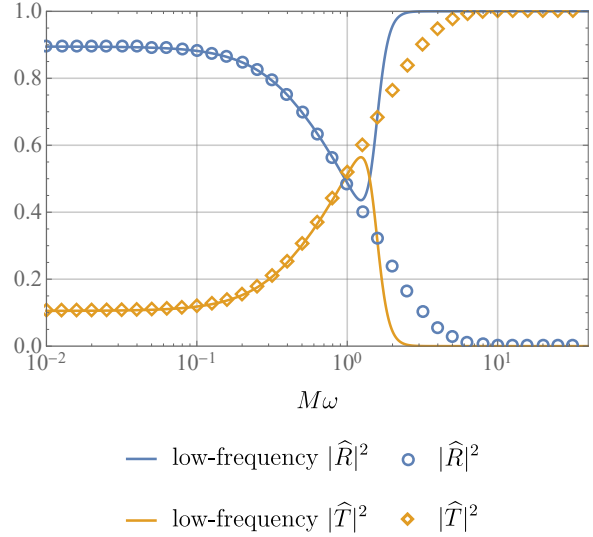


FIG. 10. A plot of $|\hat{R}|^2$ and $|\hat{T}|^2$ vs $M\omega$, obtained by evaluating a Frobenius series for each value of $M\omega$ for fixed $Q/M = 0.7$ and $l = 2$. The solid lines are the low-frequency approximations for $|\hat{R}|^2$ and $|\hat{T}|^2$, given in Eqs. 67 and 68. As expected, the low-frequency approximations break down after $M\omega \approx 1$.

will both converge at $r = M$. We use this fact to match expansions about $r = r_-$ to the expansion about $r = r_+$ which corresponds to R_{II} in Fig. 5.

We evaluated enough terms in Eqs. 71 and 74 in order to obtain 16 digits of accurate data. After matching the expansions at $r/M = 1$ for a range of values of $M\omega$ at fixed $Q/M = 0.7$ and $l = 2$, we obtained the data shown in Fig. 10. The low-frequency approximation breaks down around $M\omega \approx 1$ as expected. However, the ω^2 term under the square root in Eq. 68 is largely responsible for the breakdown of the approximation, for when we neglect this term, the approximation is rather good even at high frequencies, as seen in Fig. 11. The figure shows the difference between our numerical result and the lower limit of Eq. 49, which we can use to determine when the eigenvalues are real and when they are complex conjugate pairs of unit modulus. When $|\hat{R}|^2$ lies between the horizontal axis and the upper limit curve, the eigenvalues are complex. Otherwise, the eigenvalues are real. This can be seen in Fig. 12, where we plot the modulus of the eigenvalues. When the eigenvalues are complex, they have unit modulus. When the eigenvalues are real, they grow exponentially, approaching the high frequency limit, where $|\hat{T}|^2 \rightarrow 1$ and $\lambda_{\pm} \rightarrow (K_+/K_-)^{\pm 1} = e^{\pm 4\pi M\omega}$.

We are now in a position to answer the question posed at the end of Sec. III C 2: is it possible

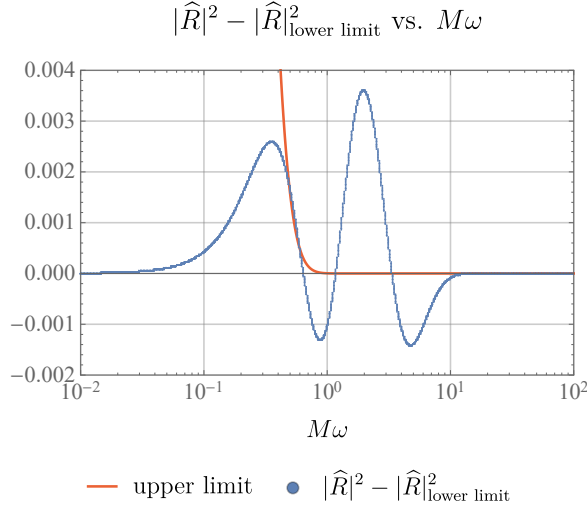


FIG. 11. The difference between our numerical series result for $|\hat{R}|^2$ and the lower limit for obtaining complex eigenvalues, shown in Eq. 49. Note that the true values of $|\hat{R}|^2$ remain near the lower limit for all $M\omega$, not just at low frequency as one might expect. Above the upper limit curve, the upper limit of Eq. 49, and below the horizontal axis, the eigenvalues of M_{++} given in Eq. 44 are real, resulting in a divergent solution space.

to construct a non-divergent, globally positive frequency solution for a maximal analytic extension of RN spacetime? The answer is yes, but only for certain ranges of $M\omega$ for fixed Q/M and l . In our case study of $Q/M = 0.7$ and $l = 2$, we can see in Fig. 12 that the only values of $M\omega$ which give non-divergent solutions are approximately $M\omega < 0.5$ and then again briefly at $M\omega \approx 0.6, 1.1, \text{ and } 3.1$. These values correspond to the regions in Fig. 11 where $|\hat{R}|^2$ lies between the horizontal axis and the upper limit. When ω takes on these values, the global solution acquires only a phase when propagating across each extended geometry, and is thus non-divergent.

V. LINEARLY INDEPENDENT AND SYMMETRIC FIELDS

The goal of this section is to build symmetric and anti-symmetric fields out of solutions with specified frequencies at each horizon. In order to do this, we first establish how many solutions are linearly independent for a geometry with n horizons, then we construct a basis, and finally we can use this basis to construct the symmetric solutions.

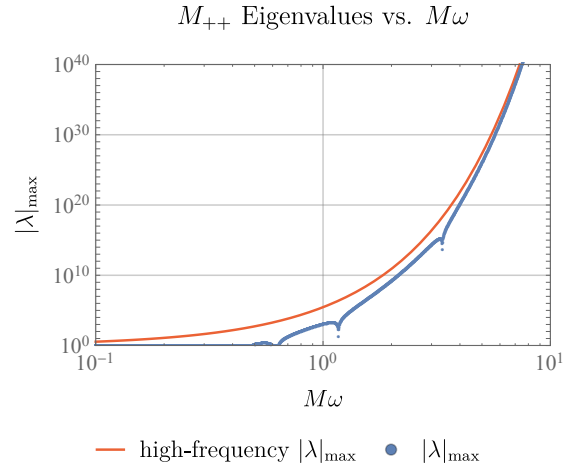


FIG. 12. A plot of the eigenvalues of M_{++} vs $M\omega$. We can see that when $|\hat{R}|^2$ lies between the lower and upper limits shown in Fig. 11, $|\lambda| = 1$, and the solution space is non-divergent. As $M\omega$ increases, $|T|^2 \rightarrow 1$, and the eigenvalues approach their high-frequency limit of $\lambda_{\pm} \rightarrow (K_+/K_-)^{\pm 1} = e^{\pm 4\pi M\omega}$. From this plot, we see that the solution space is non-divergent only for certain regions of $M\omega$.

A. Linear Independence of Positive and Negative Frequency Solutions

There are two distinctions between global solutions in extended RN which contribute to the number of linearly independent solutions. The first distinction is in the specified boundary conditions, and the second is in the choice of analytic continuation across each bifurcation point (choosing a positive- or negative-frequency solution at that horizon). In this section we sketch an induction argument, which shows that a basis of Klein-Gordon solutions in extended RN has $2(n+1)$ linearly independent solutions, where n is the number of inner and outer horizons, counted together. Equivalently, n is the number of bifurcation points in the Penrose diagram.

For the base case $n = 0$, we consider region II with no horizons. Because the Klein-Gordon equation is second-order, there are two linearly independent solutions in this region, and no analytic continuation is needed. We've proven the base case.

For the induction step, we imagine that we know there are $2(n+1)$ linearly independent solutions for a solution of n horizons linked together as shown in Fig. 3. Here we consider the case where the extended RN geometry terminates with region II, but the argument for a geometry terminating with region II' is nearly identical. Without loss of generality, we can take the solutions to be of the forms in Fig. 13. There are $n+1$ solutions of the form on the left

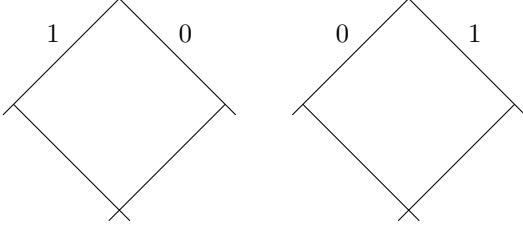


FIG. 13. A representation of $2(n+1)$ linearly independent solutions. There are $n+1$ solutions of each form.

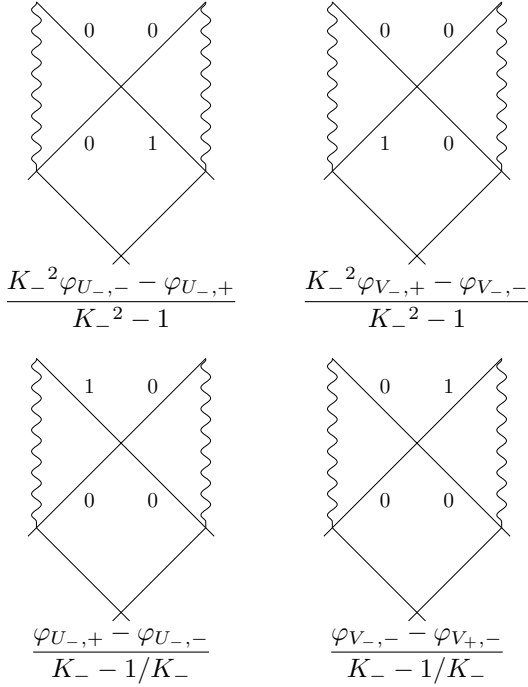


FIG. 14. A set of solutions obtained through analytic extension of those represented in Fig. 13, using the notation of Fig. 18 in Appendix A. The top two diagrams represent the original $2(n+1)$ solutions, identical to the solutions in Fig. 13, except the scattering coefficients on the new uppermost boundaries are equal to zero. The bottom two diagrams each represent the two “new” solutions, each obtained from a linear combination of analytic extensions of the old solutions.

and $n+1$ solutions of the form on the right. This specifies the boundary conditions.

Now consider an analytical extension of the geometry with an additional inner horizon. It will suffice to construct a basis of solutions for the new geometry with $2(n+2)$ independent solutions. We extend each solution with positive frequency and with negative frequency and take the linear combinations shown in Fig. 14. (See Appendix A for details on the analytic extension procedure.) The first two diagrams represent the original $2(n+1)$ solutions with the scattering coefficients on the new

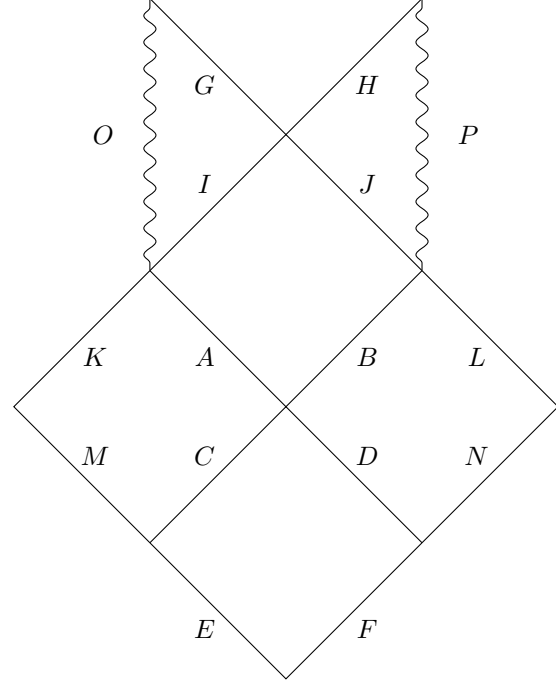


FIG. 15. An extended RN geometry with all boundaries labeled.

uppermost boundaries equal to zero. The second two diagrams have nonzero coefficients only on the new uppermost boundaries and represent the two “new” solutions obtained from the analytical extension. Because the first two diagrams are a basis for all lower boundaries (from the induction hypothesis), and the second two diagrams from a complete basis of the two new independent boundaries, this set of $2(n+2)$ solutions form a complete basis for the entire extended geometry. We’ve proved the induction step and that the Klein-Gordon equation has $2(n+1)$ linearly independent solutions for an extended RN geometry with n horizons.

B. A complete basis of solutions

In this section (see Table I for notation), we explicitly construct a basis of solutions for an extended RN geometry with $n=2$ horizons (as shown in Fig. 2), which means that there are six linearly independent solutions. The chart in Table I shows the scattering amplitudes of the solution on the corresponding boundary in Fig. 15.

One may notice that the solutions $\phi_{+,\alpha}^-$ and $\phi_{+,\beta}^-$ are missing from this basis. This is because they are not linearly independent from the other six. To see this, notice that only six of the scattering coefficients for the boundaries in Fig. 15 are not deter-

mined by scattering. Two of these six coefficients are set boundary conditions, and the other four are determined by the choice of analytic continuation at the respective horizon. We choose boundaries A , B , C , D , G , and H to be those with the six independent scattering coefficients. Since we have six linearly independent solutions, we can fully determine these six coefficients, including constructing the solutions

$\phi_{+,\alpha}^-$ and $\phi_{+,\beta}^-$.

We can write any solution ϕ for the extended RN geometry in the form

$$\phi = a\phi_{+,\alpha}^+ + b\phi_{-,\alpha}^+ + c\phi_{-,\alpha}^- + d\phi_{+,\beta}^+ + e\phi_{-,\beta}^+ + f\phi_{-,\beta}^-, \quad (75)$$

so we can find the scattering coefficients at each boundary from a matrix M :

$$\begin{pmatrix} A \\ B \\ C \\ D \\ G \\ H \end{pmatrix} = M \begin{pmatrix} a \\ b \\ c \\ d \\ e \\ f \end{pmatrix} \equiv \begin{pmatrix} 0 & 0 & 0 & 1 & 1 & 1 \\ 1 & 1 & 1 & 0 & 0 & 0 \\ 1/K_+ & K_+ & K_+ & 0 & 0 & 0 \\ 0 & 0 & 0 & K_+ & 1/K_+ & 1/K_+ \\ K_- \widehat{R}/\widehat{T} & K_- \widehat{R}/\widehat{T} & \widehat{R}/K_- \widehat{T} & K_-/\widehat{T}^* & K_-/\widehat{T}^* & 1/K_- \widehat{T}^* \\ 1/K_- \widehat{T} & 1/K_- \widehat{T} & K_-/\widehat{T} & \widehat{R}^*/K_- \widehat{T}^* & \widehat{R}^*/K_- \widehat{T}^* & K_- \widehat{R}^*/\widehat{T}^* \end{pmatrix} \begin{pmatrix} a \\ b \\ c \\ d \\ e \\ f \end{pmatrix}, \quad (76)$$

$$M^{-1} = \begin{pmatrix} 0 & \frac{K_+}{K_+ - 1/K_+} & -\frac{1}{K_+ - 1/K_+} & 0 & 0 & 0 \\ \frac{(K_- + 1/K_-)\widehat{R}^*}{(K_- - 1/K_-)\widehat{T}^{*2}} & g & \frac{1}{K_+ - 1/K_+} & 0 & -\frac{\widehat{R}^*}{(K_- - 1/K_-)\widehat{T}^*} & -\frac{1}{(K_- - 1/K_-)\widehat{T}^*} \\ -\frac{(K_- + 1/K_-)\widehat{R}^*}{(K_- - 1/K_-)\widehat{T}^{*2}} & -\frac{1/K_- + K_- |\widehat{R}|^2}{(K_- - 1/K_-)|\widehat{T}|^2} & 0 & 0 & \frac{\widehat{R}^*}{(K_- - 1/K_-)\widehat{T}^*} & \frac{1}{(K_- - 1/K_-)\widehat{T}^*} \\ -\frac{1}{K_+(K_+ - 1/K_+)} & 0 & 0 & \frac{1}{K_+ - 1/K_+} & 0 & 0 \\ -g & -\frac{(K_- + 1/K_-)\widehat{R}}{(K_- - 1/K_-)\widehat{T}^2} & 0 & -\frac{1}{K_+ - 1/K_+} & \frac{1}{(K_- - 1/K_-)\widehat{T}} & \frac{\widehat{R}}{(K_- - 1/K_-)\widehat{T}} \\ \frac{K_- + |\widehat{R}|^2/K_-}{(K_- - 1/K_-)|\widehat{T}|^2} & \frac{(K_- + 1/K_-)\widehat{R}}{(K_- - 1/K_-)\widehat{T}^2} & 0 & 0 & -\frac{1}{(K_- - 1/K_-)\widehat{T}} & -\frac{\widehat{R}}{(K_- - 1/K_-)\widehat{T}} \end{pmatrix}, \quad (77)$$

where

$$\det M = -(K_+ - 1/K_+)^2 (K_- - 1/K_-)^2, \quad (78)$$

and

$$g = \frac{(K_+/K_- - K_-/K_+)}{(K_+ - 1/K_+)(K_- - 1/K_-)|\widehat{T}|^2} + \frac{(K_+ K_- - 1/K_+ K_-)|\widehat{R}|^2}{(K_+ - 1/K_+)(K_- - 1/K_-)|\widehat{T}|^2}. \quad (79)$$

From this, we find how to express $\phi_{+,\alpha}^-$ and $\phi_{+,\beta}^-$ in terms of this basis. For example, since we know the values of the scattering coefficients of the solution $\phi_{+,\alpha}^-$, we can use Eq. 76 to find the appropriate linear

combination:

$$\begin{pmatrix} a \\ b \\ c \\ d \\ e \\ f \end{pmatrix} = M^{-1} \begin{pmatrix} 0 \\ 1 \\ 1/K_+ \\ 0 \\ \widehat{R}/K_- \widehat{T} \\ K_-/\widehat{T} \end{pmatrix} = \begin{pmatrix} 1 \\ -1 \\ 1 \\ 0 \\ 0 \\ 0 \end{pmatrix}.$$

Doing this again for $\phi_{+,\beta}^-$, we find

$$\phi_{+,\alpha}^- = \phi_{+,\alpha}^+ - \phi_{-,\alpha}^+ + \phi_{-,\alpha}^- \quad (80)$$

$$\phi_{+,\beta}^- = \phi_{+,\beta}^+ - \phi_{-,\beta}^+ + \phi_{-,\beta}^- \quad (81)$$

C. Constructing a basis of symmetric and antisymmetric solutions

Using the method outlined in the previous section, we can construct a basis of six solutions, which are

symmetric or antisymmetric at each horizon:

$$\begin{pmatrix} \phi_{s,\alpha}^s \\ \phi_{a,\alpha}^s \\ \phi_{a,\alpha}^a \\ \phi_{s,\beta}^s \\ \phi_{a,\beta}^s \\ \phi_{a,\beta}^a \end{pmatrix} = S \begin{pmatrix} \phi_{+,\alpha}^+ \\ \phi_{-,\alpha}^+ \\ \phi_{-,\alpha}^- \\ \phi_{+,\beta}^+ \\ \phi_{-,\beta}^+ \\ \phi_{-,\beta}^- \end{pmatrix}, \quad (82)$$

where the a or s indicates anti-symmetric or symmetric on the given horizon and the matrix S is given in Fig. 16. The symmetric and anti-symmetric solutions are shown explicitly in Table II.

Note that even though the upwards and downwards scattering coefficients match, one cannot simply “stack” these solutions in order to obtain symmetric solutions for an extended geometry. Instead, one must construct $2n + 2$ solutions with pure frequency at each of the n horizons, and then invert the $(2n + 2) \times (2n + 2)$ matrix representing those solutions in order to obtain the symmetric solutions. This is clearly no easy task, but is in principle possible for any finite number of horizons.

VI. DISCUSSION

While the goal of this paper is to provide the tools necessary to construct an antipodal symmetric QFT in RN, we have uncovered rich features of the Klein-Gordon equation in RN along the way. We have characterized Klein-Gordon solutions in terms of their scattering data (transmission and reflection amplitudes) in each of regions I, II, and III respectively, and used this data to construct globally positive (and negative) frequency solutions throughout the entire domain portrayed in Fig. 2. By careful choice of an initial starting point, we could characterize these solutions in terms of the surface gravity at each of the two horizons, and the scattering data arising just in region II. Motivated by this fact and an infinite analytic extension of the type shown in Fig. 3, we also sought the low frequency limits of, and numerical results for, $|\widehat{T}|$ and $|\widehat{R}|$ in order to determine the field amplitude as it propagates along the analytic extension. We found that, for low enough frequency, field amplitudes of solutions with purely positive or negative frequency at each horizon will acquire only a phase after passing both the inner and outer horizons, while at higher frequencies the amplitudes will tend to grow exponentially in one direction, and decay in the other direction.

The positive and negative frequency we have constructed lend themselves to a thermal description because their analyticity reflects periodicity in imaginary time with a temperature at each horizon fixed

by its surface gravity. This characteristic is precisely that recognized by Israel [32] to bring out the correspondence between black hole thermodynamics and the independently developed notions of thermo-field theory. This initially arose for completely different reasons but, in this context, hints at the possibility of antipodal identification, may permit a micro-canonical representation of entropy for eternal black holes [33], and leads to the possibility of generalizing the path integral approach to black-hole thermodynamics [34].

Ideas of antipodal identification were originally proposed by ’t Hooft in relation to the Schwarzschild black hole [14, 15], and lead to the specific construction of globally symmetric or antisymmetric fields under the antipodal map by others [16]. Antipodal identification is still favoured for some formulations related to quantum considerations. For quantum fields, in particular, the globally symmetric or antisymmetric constructions are best expressed in terms of the globally positive and negative frequency solutions, which can be associated with individual particle states. Here we have extended the related constructions to the Reissner-Nordström spacetime, which necessitates a somewhat richer analysis because the maximal analytic extension of the spacetime extends infinitely to the future and to the past.

Our construction has been especially oriented toward its future application to quantum fields in the maximally extended RN spacetime. As we added additional asymptotically null boundaries (or additional horizons), we necessarily increased the diversity of field configurations which needed to be considered. For an extended geometry with n horizons, we have demonstrated how to construct a basis consisting of $2(n + 1)$ linearly independent symmetric and antisymmetric fields. We have done this explicitly for $n = 2$. In order to construct this basis, we need solutions with positive frequency on some horizons and negative frequency on others. Once identified, this symmetric/antisymmetric basis could be used to begin constructing the corresponding QFT.

ACKNOWLEDGEMENTS

ATF and BFW wish to express gratitude to Gerard ’t Hooft for initially inspiring this project. ATF acknowledges partial support for this work by FCT/Portugal through UID/MAT/04459/2013, grant (GPSEinstein) PTDC/MAT-ANA/1275/2014 and SFRH/BPD/115959/2016. BFW acknowledges support from NSF grants PHY-1205906, PHY-1314529 and PHY-1607323. NAS acknowledges support from the Graduate Student Fellowship from the University of Florida.

$$S = \begin{pmatrix} \frac{K_+}{K_+ + 1} & -\frac{K_+ - K_- + |\widehat{R}|^2(1 - K_+ K_-)}{(K_+ + 1)(K_- + 1)|\widehat{T}|^2} & \frac{1 - K_- |\widehat{R}|^2}{(K_- + 1)|\widehat{T}|^2} & 0 & -\frac{(K_- - 1)\widehat{R}}{(K_- + 1)\widehat{T}^2} & \frac{(K_- - 1)\widehat{R}}{(K_- + 1)\widehat{T}^2} \\ \frac{K_+}{K_+ - 1} & -\frac{K_+ + K_- - |\widehat{R}|^2(1 + K_+ K_-)}{(K_+ - 1)(K_- + 1)|\widehat{T}|^2} & \frac{1 - K_- |\widehat{R}|^2}{(K_- + 1)|\widehat{T}|^2} & 0 & -\frac{(K_- - 1)\widehat{R}}{(K_- + 1)\widehat{T}^2} & \frac{(K_- - 1)\widehat{R}}{(K_- + 1)\widehat{T}^2} \\ \frac{K_+}{K_+ - 1} & -\frac{K_+ - K_- - |\widehat{R}|^2(1 - K_+ K_-)}{(K_+ - 1)(K_- - 1)|\widehat{T}|^2} & -\frac{(K_- - 1)\widehat{R}^*}{(K_- + 1)\widehat{T}^{*2}} & \frac{1}{K_+ + 1} & \frac{K_+ - K_- + |\widehat{R}|(1 - K_+ K_-)}{(K_+ + 1)(K_- + 1)|\widehat{T}|^2} & \frac{(K_- + 1)\widehat{R}}{(K_- + 1)|\widehat{T}|^2} \\ 0 & \frac{(K_- - 1)\widehat{R}^*}{(K_- + 1)\widehat{T}^{*2}} & -\frac{(K_- - 1)\widehat{R}^*}{(K_- + 1)\widehat{T}^{*2}} & -\frac{1}{K_+ - 1} & \frac{K_+ + K_- - |\widehat{R}|(1 + K_+ K_-)}{(K_+ - 1)(K_- + 1)|\widehat{T}|^2} & \frac{K_- - |\widehat{R}|^2}{(K_- + 1)\widehat{T}^2} \\ 0 & \frac{(K_- - 1)\widehat{R}^*}{(K_- + 1)\widehat{T}^{*2}} & -\frac{(K_- - 1)\widehat{R}^*}{(K_- + 1)\widehat{T}^{*2}} & -\frac{1}{K_+ - 1} & \frac{K_+ - K_- - |\widehat{R}|(1 - K_+ K_-)}{(K_+ - 1)(K_- - 1)|\widehat{T}|^2} & \frac{K_- + |\widehat{R}|^2}{(K_- - 1)\widehat{T}^2} \\ 0 & \frac{(K_- - 1)\widehat{R}^*}{(K_- + 1)\widehat{T}^{*2}} & -\frac{(K_- - 1)\widehat{R}^*}{(K_- + 1)\widehat{T}^{*2}} & -\frac{1}{K_+ - 1} & -\frac{K_+ - K_- - |\widehat{R}|(1 - K_+ K_-)}{(K_+ - 1)(K_- - 1)|\widehat{T}|^2} & \frac{K_- + |\widehat{R}|^2}{(K_- - 1)\widehat{T}^2} \end{pmatrix}. \quad (83)$$

FIG. 16. The change of basis matrix between pure frequency solutions and antipodal symmetric and anti-symmetric solutions.

-
- [1] E. Schrödinger, *Expanding Universe* (Cambridge University Press, Cambridge, 2011).
- [2] N. Sanchez, *Nucl. Phys.* **B294**, 1111 (1987).
- [3] G. W. Gibbons, in *Recent developments in theoretical and experimental general relativity, gravitation and relativistic field theories. Proceedings, 6th Marcel Grossmann Meeting, Kyoto, Japan, June 23-29, 1991. Pts. A, B* (1992) pp. 1013–1032.
- [4] A. O. Barvinsky, *J. Cosmol. Astropart. Phys.* **1209**, 33 (2012).
- [5] G. W. Gibbons, *Nucl. Phys.* **B271**, 497 (1986).
- [6] G. W. Gibbons and H. J. Pohle, *Nucl. Phys.* **B410**, 117 (1993).
- [7] G. W. Gibbons and S. W. Hawking, *Commun. Math. Phys.* **148**, 345 (1992).
- [8] G. W. Gibbons and C. A. R. Herdeiro, *Class. Quantum Gravity* **16**, 3619 (1999).
- [9] M. A. Castagnino, J. P. Paz, and N. G. Sanchez, *Phys. Lett.* **B193**, 13 (1987).
- [10] G. Domenech, M. L. Levinas, and N. G. Sanchez, *Int. J. Mod. Phys.* **A3**, 2567 (1988).
- [11] C. Stephens, *Ann. Phys. (N. Y.)* **193**, 255 (1989).
- [12] J. L. Friedman and A. Higuchi, *Phys. Rev.* **D52**, 5687 (1995).
- [13] Z. Chang and X. Li, *Int. J. Mod. Phys.* **A23**, 1821 (2008).
- [14] G. 't Hooft, *J. Geom. Phys.* **1**, 45 (1984).
- [15] G. 't Hooft, *Nucl. Phys.* **B256**, 727 (1985).
- [16] N. Sanchez and B. Whiting, *Nucl. Phys.* **B283**, 605 (1987).
- [17] M. Martellini and N. G. Sanchez, *Phys. Lett.* **B192**, 361 (1987).
- [18] B. F. Whiting, *Physica* **A158**, 437 (1989).
- [19] G. 't Hooft, *Found. Phys.* **46**, 1185 (2016).
- [20] G. 't Hooft, “The Quantum Black Hole as a Hydrogen Atom: Microstates Without Strings Attached,” (2016), [arXiv:1605.05119 \[gr-qc\]](https://arxiv.org/abs/1605.05119).
- [21] G. 't Hooft, *Found. Phys.* **47**, 1503 (2017).
- [22] G. 't Hooft, *Found. Phys.* **48**, 1134 (2018).
- [23] P. Betzios, N. Gaddam, and O. Papadoulaki, *J. High Energy Phys.* **2016**, 131 (2016).
- [24] A. Bzowski, A. Gnecci, and T. Hertog, *J. High Energy Phys.* **2018**, 167 (2018).
- [25] N. Sanchez, “The new quantum structure of the space-time,” (2018).
- [26] N. G. Sanchez, *Int. J. Mod. Phys.* **D28**, 1950055 (2019).
- [27] E. Poisson, *A Relativist's Toolkit: The Mathematics of Black-Hole Mechanics* (Cambridge University Press, Cambridge, 2004).
- [28] C. Kehle and Y. Shlapentokh-Rothman, *Annales Henri Poincaré* **20**, 1583 (2019).
- [29] A. Giveon, B. Kol, A. Ori, and A. Sever, *JHEP* **08**, 014 (2004), [arXiv:hep-th/0401209 \[hep-th\]](https://arxiv.org/abs/hep-th/0401209).
- [30] M. Abramowitz and I. A. Stegun, *Handbook of Mathematical Functions with Formulas, Graphs, and Mathematical Tables*, 9th ed. (Dover, New York, 1964).
- [31] C. Bender and S. Orszag, *Advanced Mathematical Methods for Scientists and Engineers I*, 1st ed. (Springer, New York, 1999).
- [32] W. Israel, *Phys. Lett.* **A57**, 107 (1976).
- [33] E. A. Martinez, *Phys. Rev.* **D51**, 5732 (1995).
- [34] V. P. Frolov and E. A. Martinez, *Class. Quantum Gravity* **13**, 481 (1996).
- [35] S. M. Carroll, *Spacetime and geometry: An introduction to general relativity* (Pearson, Harlow, 2014).

Appendix A: Positive and Negative Frequency Solutions

In developing positive- and negative-frequency solutions to the Klein-Gordon equation, we restrict our attention to the behavior of solutions near the horizons, starting with the outer horizon $r = r_+$. Using the development in Sec. III, by specifying boundary conditions in region I of Fig. 2, we can construct two linearly independent solutions $\varphi_{U_+} \approx \frac{r_+}{r} e^{i\omega(r_*-t)} Y_{lm}$ and $\varphi_{V_+} \approx \frac{r_+}{r} e^{-i\omega(r_*+t)} Y_{lm}$, which are defined near the past and future outer horizons, respectively. We can analytically extend these solutions to regions II, I', and II' by expressing them in terms of the coordinates U_+ and V_+ given in Eqs. 10 and 11:

$$\varphi_{U_+} \approx \frac{r_+}{r} U_+^{i\omega/\kappa_+} Y_{lm}, \quad (\text{A1})$$

$$\varphi_{V_+} \approx \frac{r_+}{r} V_+^{-i\omega/\kappa_+} Y_{lm}. \quad (\text{A2})$$

One can think of φ_U as waves crossing the past horizon and φ_V as waves crossing the future horizon. We would like to express φ_{U_+} and φ_{V_+} in terms of r_* and t in regions II, I' and II', which will allow us to construct global solutions. This is accomplished by specifying $-1 = e^{\pm i\pi}$ in Eqs. 10 and 11:

$$\begin{aligned} \varphi_{U_+}|_{\text{I,II}'} &= \frac{r_+}{r} |U_+|^{i\omega/\kappa_+} Y_{lm} \\ &= \frac{r_+}{r} e^{i\omega(r_*-t)} Y_{lm} \end{aligned} \quad (\text{A3})$$

$$\begin{aligned} \varphi_{U_+}|_{\text{I}',\text{II}} &= \frac{r_+}{r} (-|U_+|)^{i\omega/\kappa_+} Y_{lm} \\ &= K_+ \pm 1 \frac{r_+}{r} e^{i\omega(r_*-t)} Y_{lm} \end{aligned} \quad (\text{A4})$$

$$\begin{aligned} \varphi_{V_+}|_{\text{I,II}} &= \frac{r_+}{r} |V_+|^{-i\omega/\kappa_+} Y_{lm} \\ &= \frac{r_+}{r} e^{-i\omega(r_*+t)} Y_{lm} \end{aligned} \quad (\text{A5})$$

$$\begin{aligned} \varphi_{V_+}|_{\text{I}',\text{II}'} &= \frac{r_+}{r} (-|V_+|)^{-i\omega/\kappa_+} Y_{lm} \\ &= K_+ \mp 1 \frac{r_+}{r} e^{-i\omega(r_*+t)} Y_{lm}, \end{aligned} \quad (\text{A6})$$

where $K_+ = e^{\pi\omega/\kappa_+}$. For convenience, we absorb the factor of K_+ into the radial part of our solutions. See Fig. 17 for a graphical representation of these solutions.

It turns out that the four analytic continuations are each purely positive- or negative-frequency. The terminology is borrowed from the flat space case, where positive-frequency solutions are defined as those whose time derivative pulls out a factor of $-i\omega$ and negative-frequency solutions pull out a factor of $+i\omega$. This is not a covariant definition for the curved-space case [35]. A covariant norm definition

consistent with the flat space definition uses the following covariant inner product, which is an integral on a global, spacelike (Cauchy) surface:

$$\langle \phi, \varphi \rangle = -i \int (\phi^* \partial_\mu \varphi - \varphi \partial_\mu \phi^*) \sqrt{-g} d\Sigma^\mu, \quad (\text{A7})$$

which is invariant to the choice of surface. Positive-frequency solutions are positive-norm solutions and negative-frequency solutions are negative-norm solutions [35]. The sign of the integral in Eq. A7 is of course sensitive to the orientation of the Cauchy surface. We choose an orientation such that the normal vector points in the $\partial(V_+ - U_+)$ direction in both regions I and I' (upwards on the Penrose diagram). This results in a positive norm for all of our solutions in region I and a negative norm in region I'. The choice of sign in the exponents of Eqs. A4 and A6 determine the norm of the global solution. For either solution, we find choosing the minus sign in the exponents will result in a globally positive norm because the solution in region I' is smaller in magnitude than the solution in region I. Thus, the solution has a globally positive norm and is positive-frequency on the given horizon. Likewise, the choice of the plus sign for either solution will result in a globally negative norm and thus negative-frequency solution. Graphical representations of these solutions are in Fig. 17.

The development for analytic continuation past the inner horizon is very similar, except we use a normal vector for the Cauchy surface pointing in the $-\partial(V_- + U_-)$ direction in regions III and III' (still upwards on the Penrose diagram). Thus, solutions in region III have positive norm and solutions in region III' have negative norm. We can use this to construct the solutions in Fig. 18, analogous to those in Fig. 17.

We have constructed a global basis of solutions for behavior near the inner and outer horizons of the extended RN manifold. For the past and future horizons each, we have a positive- and negative-frequency analytical continuation to the extended manifold, for a total of four solutions per bifurcation point, represented in Fig. 17. Because we have four solutions and four boundaries at each bifurcation point, we can express a solution with arbitrary scattering amplitudes at these four boundaries in terms of purely positive- and negative-frequency solutions, a fact we use in Sec. V. We use these solutions implicitly in Sec. III C 2 to analytically continue an arbitrary solution past the bifurcation point, choosing from the positive-frequency set. We have now demonstrated how to analytically continue Klein-Gordon solutions past both the inner and outer horizons with either positive or negative frequency.

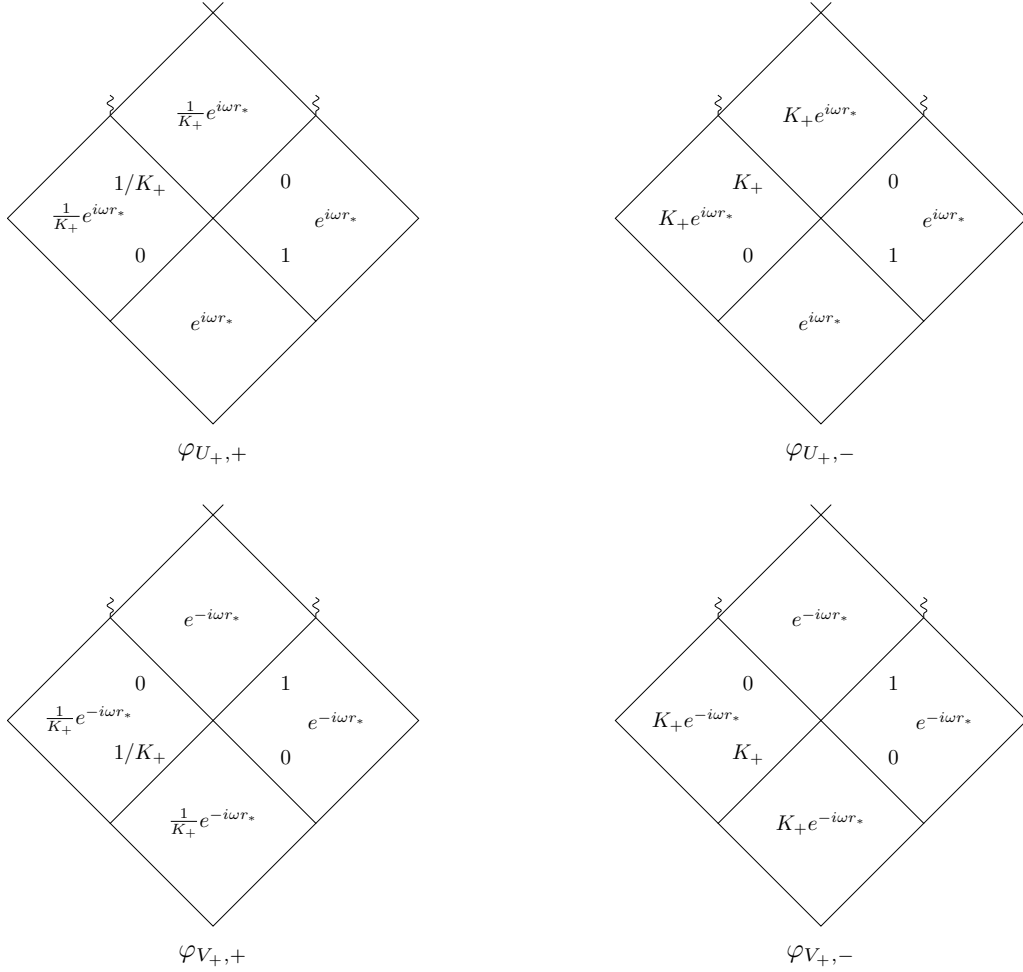


FIG. 17. Four pure-frequency Klein-Gordon solutions for the outer horizon, the U_+ or V_+ signifying the boundary conditions and the subscript \pm indicating positive- or negative-frequency. The scattering amplitudes are labeled on each horizon, and the radial part of the solution is written in the center of each region.

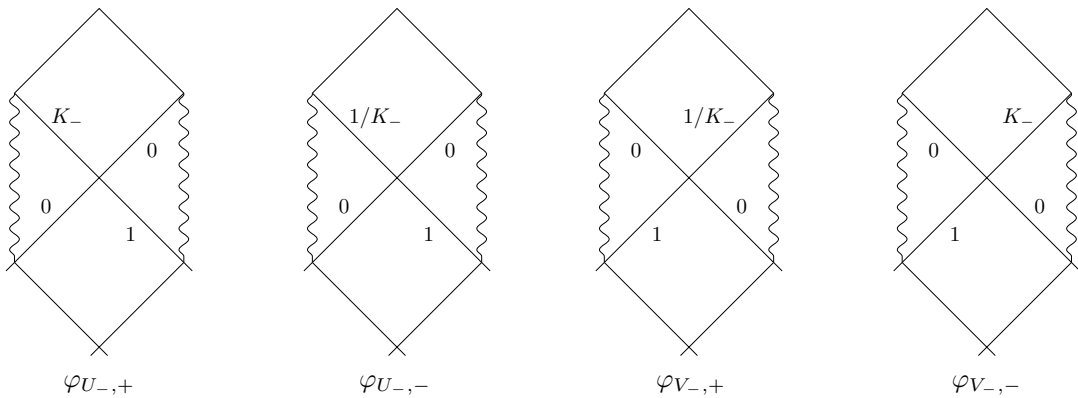


FIG. 18. Four pure-frequency Klein-Gordon solutions for the inner horizon, the U_- or V_- signifying the boundary conditions and the subscript \pm indicating positive- or negative-frequency. The scattering amplitudes are labeled on each horizon.

	$\phi_{+,\alpha}^+$	$\phi_{-,\alpha}^+$	$\phi_{+,\alpha}^-$	$\phi_{-,\alpha}^+$	$\phi_{+,\beta}^+$	$\phi_{-,\beta}^+$	$\phi_{+,\beta}^-$	$\phi_{-,\beta}^-$
A	0	0	0	1	1	1	1	1
B	1	1	1	0	0	0	0	0
C	$1/K_+$	K_+	K_+	0	0	0	0	0
D	0	0	0	K_+	$1/K_+$	$1/K_+$	$1/K_+$	$1/K_+$
E	$\hat{R}/K_+\hat{T}$	$K_+\hat{R}/\hat{T}$	$K_+\hat{R}/\hat{T}$	$K_+\hat{R}/\hat{T}$	$1/K_+\hat{T}^*$	$1/K_+\hat{T}^*$	$1/K_+\hat{T}^*$	$1/K_+\hat{T}^*$
F	$1/K_+\hat{T}$	K_+/\hat{T}	$K_+\hat{R}^*/\hat{T}^*$	$\hat{R}^*/K_+\hat{T}^*$	$\hat{R}^*/K_+\hat{T}^*$	$\hat{R}^*/K_+\hat{T}^*$	$\hat{R}^*/K_+\hat{T}^*$	$\hat{R}^*/K_+\hat{T}^*$
G	$K_-\hat{R}/\hat{T}$	$K_-\hat{R}/\hat{T}$	$\hat{R}/K_-\hat{T}$	$K_-\hat{T}^*$	$K_-\hat{T}^*$	$K_-\hat{T}^*$	$1/K_-\hat{T}^*$	$1/K_-\hat{T}^*$
H	$1/K_-\hat{T}$	$1/K_-\hat{T}$	$K_-\hat{T}$	$\hat{R}^*/K_-\hat{T}^*$	$\hat{R}^*/K_-\hat{T}^*$	$\hat{R}^*/K_-\hat{T}^*$	$K_-\hat{R}^*/\hat{T}^*$	$K_-\hat{R}^*/\hat{T}^*$
I	$1/\hat{T}$	$1/\hat{T}$	$1/\hat{T}$	\hat{R}^*/\hat{T}^*	\hat{R}^*/\hat{T}^*	\hat{R}^*/\hat{T}^*	\hat{R}^*/\hat{T}^*	\hat{R}^*/\hat{T}^*
J	\hat{R}/\hat{T}	\hat{R}/\hat{T}	\hat{R}/\hat{T}	$1/\hat{T}^*$	$1/\hat{T}^*$	$1/\hat{T}^*$	$1/\hat{T}^*$	$1/\hat{T}^*$
K	$1/K_+T$	K_+T	K_+T	R^*/T^*	R^*/T^*	R^*/T^*	R^*/T^*	R^*/T^*
L	R/T	R/T	R/T	K_+T^*	$1/K_+T^*$	$1/K_+T^*$	$1/K_+T^*$	$1/K_+T^*$
M	R/K_+T	K_+R/T	K_+R/T	$1/T^*$	$1/T^*$	$1/T^*$	$1/T^*$	$1/T^*$
N	$1/T$	$1/T$	$1/T$	K_+R^*/T^*	R^*/K_+T^*	R^*/K_+T^*	R^*/K_+T^*	R^*/K_+T^*
	$\frac{K_-\hat{R}B^*-B}{i\hat{T}/2\omega r_+}$	$\frac{K_-\hat{R}B^*-B}{i\hat{T}/2\omega r_+}$	$\frac{\hat{R}B^*/K_--B}{i\hat{T}/2\omega r_+}$	$\frac{K_--\hat{R}^*B}{i\hat{T}^*/2\omega r_+}$	$\frac{K_--\hat{R}^*B}{i\hat{T}^*/2\omega r_+}$	$\frac{K_--\hat{R}^*B}{i\hat{T}^*/2\omega r_+}$	$\frac{B^*/K_--\hat{R}^*B}{i\hat{T}^*/2\omega r_+}$	$\frac{B^*/K_--\hat{R}^*B}{i\hat{T}^*/2\omega r_+}$
O	$-\frac{K_-\hat{R}A^*-A}{i\hat{T}/2\omega r_+}$	$-\frac{K_-\hat{R}A^*-A}{i\hat{T}/2\omega r_+}$	$-\frac{\hat{R}A^*/K_--A}{i\hat{T}/2\omega r_+}$	$-\frac{K_--\hat{R}^*A}{i\hat{T}^*/2\omega r_+}$	$-\frac{K_--\hat{R}^*A}{i\hat{T}^*/2\omega r_+}$	$-\frac{K_--\hat{R}^*A}{i\hat{T}^*/2\omega r_+}$	$-\frac{A^*/K_--\hat{R}^*A}{i\hat{T}^*/2\omega r_+}$	$-\frac{A^*/K_--\hat{R}^*A}{i\hat{T}^*/2\omega r_+}$
	$\frac{K_-\hat{R}B^*-B}{i\hat{T}K_-/2\omega r_+}$	$\frac{K_-\hat{R}B^*-B}{i\hat{T}K_-/2\omega r_+}$	$\frac{\hat{R}B^*-BK_-}{i\hat{T}/2\omega r_+}$	$\frac{K_--\hat{R}^*B}{i\hat{T}^*K_-/2\omega r_+}$	$\frac{K_--\hat{R}^*B}{i\hat{T}^*K_-/2\omega r_+}$	$\frac{K_--\hat{R}^*B}{i\hat{T}^*K_-/2\omega r_+}$	$\frac{B^*-K_--\hat{R}^*B}{i\hat{T}^*/2\omega r_+}$	$\frac{B^*-K_--\hat{R}^*B}{i\hat{T}^*/2\omega r_+}$
P	$-\frac{K_-\hat{R}A^*-A}{i\hat{T}K_-/2\omega r_+}$	$-\frac{K_-\hat{R}A^*-A}{i\hat{T}K_-/2\omega r_+}$	$-\frac{\hat{R}A^*-K_--A}{i\hat{T}/2\omega r_+}$	$-\frac{K_--\hat{R}^*A}{i\hat{T}^*K_-/2\omega r_+}$	$-\frac{K_--\hat{R}^*A}{i\hat{T}^*K_-/2\omega r_+}$	$-\frac{K_--\hat{R}^*A}{i\hat{T}^*K_-/2\omega r_+}$	$-\frac{A^*-K_--\hat{R}^*A}{i\hat{T}^*/2\omega r_+}$	$-\frac{A^*-K_--\hat{R}^*A}{i\hat{T}^*/2\omega r_+}$

TABLE I. Six solutions that form a complete basis for an extended RN geometry. The upper sign indicates the frequency on the inner horizon, and the lower sign indicates the frequency on the upper horizon. The boundary conditions are applied in region II, and the two distinct conditions are signified by α and β . The letters A through P in the first column corresponds to the boundary in Fig. 15, and the table entries give the scattering coefficient of the corresponding boundary and solution.

	$\phi_{s,\alpha}^s$	$\phi_{a,\alpha}^s$	$\phi_{a,\alpha}^a$	$\phi_{s,\beta}^s$	$\phi_{a,\beta}^s$	$\phi_{a,\beta}^a$
<i>A</i>	0	0	0	1	1	1
<i>B</i>	1	1	1	0	0	0
<i>C</i>	1	-1	-1	0	0	0
<i>D</i>	0	0	0	1	-1	-1
<i>E</i>	\widehat{R}/\widehat{T}	$-\widehat{R}/\widehat{T}$	$-\widehat{R}/\widehat{T}$	$1/\widehat{T}^*$	$-1/\widehat{T}^*$	$-1/\widehat{T}^*$
<i>F</i>	$1/\widehat{T}$	$-1/\widehat{T}$	$-1/\widehat{T}$	$\widehat{R}^*/\widehat{T}^*$	$-\widehat{R}^*/\widehat{T}^*$	$-\widehat{R}^*/\widehat{T}^*$
<i>G</i>	\widehat{R}/\widehat{T}	\widehat{R}/\widehat{T}	$-\widehat{R}/\widehat{T}$	$1/\widehat{T}^*$	$1/\widehat{T}^*$	$-1/\widehat{T}^*$
<i>H</i>	$1/\widehat{T}$	$1/\widehat{T}$	$-1/\widehat{T}$	$\widehat{R}^*/\widehat{T}^*$	$\widehat{R}^*/\widehat{T}^*$	$-\widehat{R}^*/\widehat{T}^*$
<i>I</i>	$1/\widehat{T}$	$1/\widehat{T}$	$1/\widehat{T}$	$\widehat{R}^*/\widehat{T}^*$	$\widehat{R}^*/\widehat{T}^*$	$\widehat{R}^*/\widehat{T}^*$
<i>J</i>	\widehat{R}/\widehat{T}	\widehat{R}/\widehat{T}	\widehat{R}/\widehat{T}	$1/\widehat{T}^*$	$1/\widehat{T}^*$	$1/\widehat{T}^*$
<i>K</i>	$1/T$	$-1/T$	$-1/T$	R^*/T^*	R^*/T^*	R^*/T^*
<i>L</i>	R/T	R/T	R/T	$1/T^*$	$-1/T^*$	$-1/T^*$
<i>M</i>	R/T	$-R/T$	$-R/T$	$1/T^*$	$1/T^*$	$1/T^*$
<i>N</i>	$1/T$	$1/T$	$1/T$	R^*/T^*	$-R^*/T^*$	$-R^*/T^*$
<i>O</i>	$\frac{B^*\widehat{R}-B}{i\widehat{T}/2r_+\omega}$ $-\frac{A^*\widehat{R}-A}{i\widehat{T}/2r_+\omega} \frac{r}{r_-}$	$\frac{B^*\widehat{R}-B}{i\widehat{T}/2r_+\omega}$ $-\frac{A^*\widehat{R}-A}{i\widehat{T}/2r_+\omega} \frac{r}{r_-}$	$-\frac{B^*\widehat{R}+B}{i\widehat{T}/2r_+\omega}$ $+\frac{A^*\widehat{R}+A}{i\widehat{T}/2r_+\omega} \frac{r}{r_-}$	$\frac{B^*-B\widehat{R}^*}{i\widehat{T}^*/2r_+\omega}$ $-\frac{A^*-A\widehat{R}^*}{i\widehat{T}^*/2r_+\omega} \frac{r}{r_-}$	$\frac{B^*-B\widehat{R}^*}{i\widehat{T}^*/2r_+\omega}$ $-\frac{A^*-A\widehat{R}^*}{i\widehat{T}^*/2r_+\omega} \frac{r}{r_-}$	$-\frac{B^*+B\widehat{R}^*}{i\widehat{T}^*/2r_+\omega}$ $+\frac{A^*+A\widehat{R}^*}{i\widehat{T}^*/2r_+\omega} \frac{r}{r_-}$
<i>P</i>	$\frac{B^*\widehat{R}-B}{i\widehat{T}/2r_+\omega}$ $-\frac{A^*\widehat{R}-A}{i\widehat{T}/2r_+\omega} \frac{r}{r_-}$	$\frac{B^*\widehat{R}+B}{i\widehat{T}/2r_+\omega}$ $-\frac{A^*\widehat{R}+A}{i\widehat{T}/2r_+\omega} \frac{r}{r_-}$	$\frac{B^*\widehat{R}+B}{i\widehat{T}/2r_+\omega}$ $-\frac{A^*\widehat{R}+A}{i\widehat{T}/2r_+\omega} \frac{r}{r_-}$	$\frac{B^*-B\widehat{R}^*}{i\widehat{T}^*/2r_+\omega}$ $-\frac{A^*-A\widehat{R}^*}{i\widehat{T}^*/2r_+\omega} \frac{r}{r_-}$	$\frac{B^*-B\widehat{R}^*}{i\widehat{T}^*/2r_+\omega}$ $-\frac{A^*-A\widehat{R}^*}{i\widehat{T}^*/2r_+\omega} \frac{r}{r_-}$	$\frac{B^*+B\widehat{R}^*}{i\widehat{T}^*/2r_+\omega}$ $-\frac{A^*+A\widehat{R}^*}{i\widehat{T}^*/2r_+\omega} \frac{r}{r_-}$

TABLE II. Six solutions, which are antisymmetric (signified by *a*) or symmetric (signified by *s*) at each horizon. The upper letter is the type of symmetry on the inner horizon, and the lower letter is the type of symmetry on the outer horizon. The α or β signifies the boundary condition chosen in region II, as in the solutions shown in Table I. The letters *A* through *P* in the first column correspond to the boundary in Fig. 15, and the table entries give the scattering coefficient of the corresponding boundary and solution.